Ocean Sci. Discuss., https://doi.org/10.5194/os-2018-168
Manuscript under review for journal Ocean Sci.
Discussion started: 17 January 2019

Ocean Science Discussions
Open Access

Skill assessment of global, regional and coastal circulation forecast models: evaluating the benefits of dynamical downscaling in IBI surface waters.

Pablo Lorente[1], Marcos García-Sotillo[1], Arancha Amo-Baladrón[1], Roland Aznar[1], Bruno Levier[2], José Carlos Sánchez-Garrido[3], Simone Sammartino[3], Álvaro De Pascual[1], Guillaume Reffray[2], Cristina Toledano[1] and Enrique Álvarez-Fanjul[1]

[1]{Puertos del Estado, Madrid, Spain}

[2]{Mercator Ocean, Toulouse, France}

[3]{Physical Oceanography Group of University of Málaga (GOFIMA), Málaga, Spain}

Correspondence to: P. Lorente (plorente@puertos.es)

Abstract

In this work, a multi-parameter inter-comparison of diverse ocean forecast models was conducted at the sea surface, ranging from global to local scales in a two-phase strategy. Firstly, a comparison of CMEMS-GLOBAL and the nested CMEMS-IBI regional system was performed against satellite-derived and in situ observations. Results highlighted the overall benefits of both the GLOBAL data assimilation in open-waters and the increased horizontal resolution of IBI in coastal areas, respectively. Besides, IBI proved to capture shelf dynamics by better representing the horizontal extent and strength of a river freshwater plume, according to the results derived from the validation against in situ observations from a buoy moored in NW Spain. Secondly, a multi-model inter-comparison exercise for 2017 was performed in the Strait of Gibraltar among GLOBAL, IBI and the nested SAMPA high-resolution coastal forecast system in order to elucidate the accuracy of each system to characterize the Atlantic Jet (AJ) inflow dynamic. A quantitative validation against High Frequency radar (HFR) hourly currents highlighted both the steady improvement in AJ representation in terms of speed and direction when zooming from global to coastal scales though a multi-nesting model approach and also the relevance of a variety of factors at local scale such as a refined horizontal resolution, a tailored bathymetry and a higher spatio-temporal resolution of the atmospheric forcing. The ability of each model to reproduce a 2-day quasi-permanent full reversal of the AJ surface inflow was examined in terms of wind-induced circulation patterns. SAMPA appeared to better reproduce the reversal events detected with HFR estimations, demonstrating the potential added value of coastal models with respect to coarser parent regional systems. Finally, SAMPA coastal model outputs were also qualitatively analysed in the Western Alboran Sea to put in a broader perspective the context of the onset, development and end of such flow reversal episodes.

Keywords: forecasting; model; inter-comparison; validation, downscaling; HF radar; skill assessment;

Ocean Sci. Discuss., https://doi.org/10.5194/os-2018-168
Manuscript under review for journal Ocean Sci.
Discussion started: 17 January 2019

1 Introduction

Over the last three decades, significant progresses have been made in the discipline of operational oceanography thanks to the substantial increase in high-performance computational resources, which has fostered the seamless evolution in ocean modelling techniques and numerical efficiency (Cotelo et al., 2017) and given rise to an inventory of operational ocean forecasting systems (OOFSs) running in overlapping regions in order to reliably portray and predict the ocean state and its variability at diverse spatio-temporal scales.

Global circulation models have been steadily evolving in terms of complexity, horizontal resolution refinement and process parameterisation (Holt et al., 2017). Notwithstanding, such development involves compromises of scale and is subject to practical limits on the feasible spatial resolution (Greenberg et al., 2007). Although large-scale processes and physical and biogeochemical cycles are properly resolved by the current state-of-the-art global models resolution (e.g. nominal 1/12º), coastal and shelf phenomena are still poorly replicated or even misrepresented as the grid mesh is too coarse, especially for complex-geometry regions such as sea straits, archipelagos or semi-enclosed seas where the coastline, seamounts and bottom topography are not well resolved. In this context, tides, vertical coordinates, mixing schemes, river inflows and atmospheric forcings have been traditionally identified as five areas of further research in global ocean modelling (Holt et al., 2017).

Since the continental shelf is affected not only by natural agents (land-sea breezes, riverine discharges, bottom topography, coastline shape, etc.) but also by human-induced factors, an increased understanding of coastal circulation is essential for decision- and policy-making in the socioeconomically vital and often environmentally stressed coastal regions. Therefore, small-scale ocean features must be explicitly computed and accurately reproduced by means of regional models with finer horizontal grid spacing but for a particular delimited area. The success of this approach requires the seamless progress in several aspects, as previously identified by Kourafalou et al. (2015): i) a deep comprehension of the primary mechanisms driving coastal circulation; ii) downscaling methods to adequately represent air-sea and land-sea interactions; iii) robust methods to embed high-resolution models in coarser-scale systems. Therefore, this approach implies the transfer of large-scale information from the global model to the interior of the nested regional domain by means of diverse methodologies. One of them is the so-called 'spectral nudging' technique, adopted to ensure that the prevailing global conditions are not degraded in the open-ocean, while allowing sub-mesoscale processes to be resolved exclusively by the embedded model in the continental shelf and coastal areas (Herbert et al., 2014). Additionally, the regional modelling strategy can include some fine-tuning of physical parameters, individually tailored to each chosen area, instead of the universally valid parameterizations associated with global OOFSs.

The benefits of regional modelling over the driving global OOFS are generally assumed, but to date only few studies have explored and quantified the potential added value of such approach (Katavouta and Thomson, 2016; Rockel, 2015; Greenberg et al., 2007). The 'parent-son' model inter-comparison is mandatory during both implementation and operational stages since it aids to: i) verify the most adequate nesting strategy; ii) check the consistency of the nested model solution; and iii) identify any potential problem that might be inherited from the coarser system.

In the framework of the Copernicus Marine Environment Monitoring Service (CMEMS), a global ocean model together with a wealth of nested regional OOFSs are currently running in different areas of the European seas and providing paramount oceanographic forecast

Ocean Sci. Discuss., https://doi.org/10.5194/os-2018-168
Manuscript under review for journal Ocean Sci.
Discussion started: 17 January 2019

products (Le Traon et al., 2018). Since the validation of OOFSs against independent measurements constitutes a core activity in oceanographic operational centres, the skill of Iberia-Biscay-Ireland (IBI) regional OOFS is routinely assessed by means of the NARVAL (North Atlantic Regional VALidation) system (Sotillo et al. 2015), a web-based toolbox that provides a series of skill metrics automatically computed and delivered in the QUality Information Document - QUID - (Sotillo et al., 2014). In this context, the first goal of this paper is to conduct a multi-parameter model inter-comparison between IBI regional OOFS and the coarser parent system, the CMEMS GLOBAL (Lellouche et al., 2018), with the aim of assessing their performance at the upper-layer. Their predictive skills to properly represent the surface temperature (SST) over IBI coverage domain and diverse sub-regions were evaluated by means of comparisons against remote-sensed and in situ observations. On the other hand, their prognostic capabilities to accurately reproduce the coastal surface circulation were assessed through the analysis of a single impulsive-type river outflow episode that took place in March 2018 in the Galician coast (NW Spain), a region of freshwater influence - ROFI- (Simpson, 1997).

Despite the recent advances in the development of CMEMS global and regional core products, many downstream services for user uptake require information on even smaller spatial scale, such as ocean forecasting for small island chains (Caldeira et al., 2016), intricate bights (Stanev et al., 2016) or port approach areas where sharp topo-bathymetric gradients pose special difficulties for accurate local predictions (Sotillo et al. 2018, under review; Hlevca et al., 2018; Federico et al., 2017; Sánchez-Arcilla et al., 2016; Sammartino et al., 2014; Grifoll et al., 2012). A variety of operational products for harbours have been recently developed, although most of these coastal applications are wave and water-level forecasting systems (Lin et al., 2008; Pérez et al., 2013). By contrast, lower attention has being devoted to harbour hydrodynamic conditions since its reduced dimensions and intricate layout confer upon harbour restrictions, which are not present in the open sea. Besides, derivative products based on current forecasts, such as float trajectories, residence time maps, flushing patterns and risk assessment of water quality degradation can constitute additional assets for efficient harbour management (Álvarez-Fanjul et al., 2018; Sammartino et al., 2018). In order to overcome the existing gap between the scales effectively solved by the regional OOFSs and the coastal scales required to meet strong societal needs in support of blue and green growth, a number of downstream services are currently adopting different downscaling approaches. Dynamical downscaling takes regional boundary conditions to drive a high-resolution limited-area model in which coastal processes are calculated on a finer grid by resolving well-known hydrodynamic equations. However, uncertainties in the downscaling process are hard to quantify since coastal solutions are still exchanging poorly controlled information with larger-scale at their boundaries (Hernández et al., 2018).

As a representative example of downstream service developed by Puertos del Estado (PdE) in a hot spot area like the Strait of Gibraltar (GIBST), the operational PdE-SAMPA high-resolution coastal system (Sánchez-Garrido et al., 2013) is dynamically embedded in IBI and nowadays employed by the Port Authority of Algeciras Bay as predictive tool to support maritime policy and assist high-stakes decision-making related to marine safety, port operation optimization and mitigation of both natural disasters and anthropogenic hazards. Previous researches have unequivocally proved the ability of PdE-SAMPA to accurately capture basic circulation features of the GIBST area and Algeciras Bay (Sanchez-Garrido et al., 2014; Sammartino et al., 2014; Soto-Navarro et al., 2016). A preliminary model skill assessment was conducted within the framework of MEDESS-4MS project (Sotillo et al., 2016-a). However, the added value of this coastal OOFS with respect to its parent regional

Ocean Sci. Discuss., https://doi.org/10.5194/os-2018-168
Manuscript under review for journal Ocean Sci.
Discussion started: 17 January 2019

system IBI was only quantified from a lagrangian perspective by using a wealth of drifters. The second goal of this contribution is thus to build up upon previous model inter-comparison exercises, placing special emphasis on the characterization of the Atlantic Jet (AJ) inflow into the Mediterranean Sea in terms of speed and direction. This geostrophically adjusted jet fluctuates in a wide range of temporal scales and drives the main circulation in the Alboran Sea, feeding and surrounding the Western Alboran Gyre -WAG- (Macias et al., 2016). An inter-comparison exercise was conducted for 2017 among a global configuration (CMEMS GLOBAL), a regional application (CMEMS IBI) and a higher resolution coastal system (PdE-SAMPA), in order to characterize the AJ dynamics and their ability to adequately capture an extreme event: the quasi-permanent (up to ~48 h long) full reversal of the AJ surface flow under intense and prolonged easterlies. To this end, a High-Frequency radar (HFR) has been used as benchmark since it regularly provides quality-controlled hourly maps of the surface currents of the Strait (Lorente et al., 2014).

In summary, this paper serves one primary purpose: performing a multi-parameter model skill assessment in IBI surface waters, ranging from global to local scales in a two-phase strategy: i) a comparison between GLOBAL and IBI regional systems in the entire overlapping coverage domain, posing special attention on regionalization; and ii) a process-based multi-model inter-comparison for 2017 with a focus on the GIBST. It is worth mentioning that the present model inter-comparison is limited to the surface layer.

This paper is organized as follows: Section 2 provides further details about the study areas. Section 3 describes the diverse models configuration. Section 4 outlines the observational data sources and methodology used in this study. Sections 5 and 6 present a detailed discussion of the results. Finally, main conclusions are summarized in Section 7.

2 Study Areas

2.1 IBI area (and subregions)

From a pure physical oceanographic point of view, the IBI geographical domain is a very complex region (Figure 1, a), marked by a generally steep slope separating the deep ocean from the shelf. The western, and deeper, side of the IBI domain is affected by main large-scale currents, mainly the closure of the North Atlantic Drift, here split into two major branches, the major one continuing northwards along the north-western European shelves (NAC and NADC) and the other, the Azores Current (AC), which follows south-eastwards and has continuity in the Canary Current (CaC). On the other hand, along the slope, a poleward slope current flows in the subsurface; it is observed as far north as at Ireland latitudes. Instabilities in this slope current favour the occurrence of slope water oceanic eddies, along the northern Iberian coast (Pingree & Le Cann 1992). On the continental shelves, intense tidal motions provide the dominant source of energy (Álvarez-Fanjul et al. 1997): noticeable tidal mixing fronts arise on the most energetic tidal areas of the IBI region (i.e. English Channel, Celtic and Irish Sea). Shelf and coastal areas of the region are also affected by strong storm surges (Pérez et al. 2012). Along the western Iberian and African coasts, strong summer upwelling of bottom cold and enriched waters take place under predominant northerly wind conditions that trigger the Ekman-driven offshore deflection of the surface flux.

IBI is also a rather broad and heterogeneous area. In order to gain insight into the model skill assessment (as later exposed in Section 5), IBI service (IBISR) regional domain has been split in nine different subregions (Figure 1-a): the Irish Sea (IRISH), the English Channel

(ECHAN), the Gulf of Biscay (GOBIS), the North Iberian Shelf (NIBSH), the West Iberian Shelf (WIBSH), the Western Mediterranean Sea (WSMED), the Gulf of Cadiz (CADIZ), the Strait of Gibraltar (GIBST) and the Canarias Islands (ICANA).

2.2 Strait of Gibraltar

The Strait of Gibraltar (GIBST), the only connection between the semi-enclosed Mediterranean basin and the open Atlantic Ocean, is characterized by a two-layer baroclinic exchange which is hydraulically controlled at Camarinal Sill (Figure 1, b). Whilst saltier Mediterranean water flows out at depth, an eastward surface jet of relatively fresh Atlantic water (AJ) flows into the Alboran Sea by surrounding the quasi-permanent Western Anticyclonic Gyre (WAG) and the more elusive Eastern Anticyclonic Gyre (EAG) in a wavelike path. As the WAG owes its existence to the input of new Atlantic waters provided by the AJ, both structures are widely considered to be coupled and usually referred as to the AJ-WAG system. A significant variety of analytical, field and modelling studies have previously attempted to disentangle the AJ-WAG system and properly explain the underlying physical processes (Sánchez-Garrido et al., 2013; Macías et al., 2007-a; Viúdez, 1997).

The position, intensity and direction of the AJ fluctuate in a broad range of temporal scales, driving the upper-layer circulation of the Alboran Sea with subsequent physical and biological implications (Solé et al, 2016; Sánchez-Garrido et al. 2015; Ruiz et al., 2013). For instance, the presence of a strong AJ close to the northern shore of the Alboran Sea reinforces the coastal upwelling and therefore increases both the near-shore chlorophyll concentration and the spawning of fish in this region (Ruiz et al., 2013; Macías et al., 2008). By contrast, meteorologically-induced inflow interruptions can trigger the weakening and even the decoupling of the AJ-WAG system (Sánchez-Garrido et al., 2013), the subsequent eastward migration of the WAG and the genesis of a new gyre that coexists with the other two, giving rise to a three-anticyclonic-gyre situation (Viúdez et al., 1998).

Within this context, the AJ pattern has been described to oscillate between two main circulation modes at seasonal scale (Vargas-Yáñez et al., 2002): i) a stronger AJ flows north-eastwards during the first half of the year and ii) a weaker AJ flows more southwardly towards the end of the year. Sea level Pressure (SLP) variations over the Western Mediterranean basin and local zonal wind (U) fluctuations in the Alboran Sea have been usually considered as the main factors controlling and modulating the AJ variability (Macías et al., 2007-b; Lafuente et al., 2002). In particular, the second parameter has been largely invoked as the primary driving agent to explain both the intensification of the surface inflow during prevalent westerlies and also extreme AJ collapse events recorded when intense easterlies are predominant (Macías et al., 2016). The zonal wind intensity has been reported to follow an annual cycle with more westerly (easterly) winds during winter (summer) months (Dorman et al., 1995). The seasonal variability and occasional interruptions of the Atlantic inflow due to meteorological forcing have been earlier investigated with in situ data from fixed moorings (García-Lafuente, 2002). More recently, a considerable number of satellite tracked drifters were released on both sides of GIBST within the framework of MEDESS-4MS project, providing hence a complete Lagrangian view of the Atlantic waters inflow into the Alboran Sea (Sotillo et al., 2016-b).

Ocean Sci. Discuss., https://doi.org/10.5194/os-2018-168
Manuscript under review for journal Ocean Sci.
Discussion started: 17 January 2019

3 Models description

Whereas basic features of the three OOFSs employed in this work are gathered in Table 1, further details are provided in the following devoted sub-sections.

3.1 CMEMS GLOBAL system

The Operational Mercator global ocean analysis and forecast system provides 10 days of 3D global ocean forecasts updated daily. This product includes daily mean files of temperature, salinity, currents, sea level, mixed layer depth and ice parameters from the surface to seafloor over the global ocean. It also includes hourly mean surface fields for sea level height, temperature and currents. The global ocean output files are displayed with a 1/12 degree horizontal resolution with regular longitude/latitude equirectangular projection. 50 vertical levels span from 0 to 5500 meters.

The system is based on the Nucleus for European Modelling of the Ocean (NEMO) v3.1 ocean model (Madec, 2008). The physical configuration is based on the tripolar ORCA grid type with a horizontal resolution of 9 km at the equator, 7 km at Cape Hatteras (mid-latitudes) and 2 km toward the Ross and Weddell seas. The 50-level vertical discretization retained for this system has 1 m resolution at the surface decreasing to 450 m at the bottom, and 22 levels within the upper 100 m. The bathymetry used in the system is a combination of interpolated ETOPO1 and GEBCO8 databases. The system was initialized on 11 October 2006 based on the temperature and salinity profiles from the EN4 monthly gridded climatology. The atmospheric fields forcing the ocean model are taken from the ECMWF (European Centre for Medium-Range Weather Forecasts) Integrated Forecast System. A 3-h sampling is used to reproduce the diurnal cycle. The system does not include neither tides nor pressure forcing. The monthly runoff climatology is built with data on coastal runoffs and 100 major rivers from the Dai et al (2009) database (Lellouche et al., 2018). Altimeter data, in situ temperature and salinity vertical profiles and satellite sea surface temperature are jointly assimilated to estimate the initial conditions for numerical ocean forecasting. Moreover, satellite sea ice concentration is now assimilated in the system in a monovariate/monodata mode. Further details can be found in Lellouche et al., (2018).

3.2 CMEMS IBI regional system

The IBI OOFS provides a real-time short-term 5-day hydrodynamic 3D forecast (and one day of hindcast as best estimate) of a range of physical parameters (currents, temperature, salinity and sea level) since 2011 (Sotillo et al., 2015). IBI is based on an eddy-resolving NEMO model application (v3.6) that includes high-frequency processes required to characterize regional-scale marine processes. The model application is run at 1/36º horizontal resolution and final products are routinely delivered in a service domain extending between 19ºW-5ºE and 26ºN-56ºN. The NEMO model (Madec, 2008) solves the three-dimensional finite-difference primitive equations in spherical coordinates discretized on an Arakawa-C grid and 50 geopotential vertical levels (z coordinate), assuming hydrostatic equilibrium and Boussinesq approximation. Partial bottom cell representation of the bathymetry (a composite of ETOPO 2 and GEBCO8) allows an accurate representation of the steep slopes characteristic of the area. The model grid is a subset of the Global 1/12° ORCA tripolar grid used by the parent system (the CMEMS GLOBAL system) that provides initial and lateral boundary conditions, but refined at 1/36° horizontal resolution.

The IBI run is forced every 3 hours with up-to-date high-frequency (1/8º horizontal grid resolution) meteorological forecasts (10-m wind, surface pressure, 2-m temperature, relative humidity, precipitations, shortwave and longwave radiative fluxes) provided by ECMWF.

CORE empirical bulk formulae (Large and Yeager, 2004) are used to compute latent sensible heat fluxes, evaporation and surface stress. Lateral open boundary data are interpolated from the daily outputs of the GLOBAL system. These are complemented by 11 tidal harmonics built from FES2004 (Lyard et al., 2006) and TPXO7.1 (Egbert and Erofeeva, 2002) tidal models solutions. Fresh water river discharge inputs are implemented as lateral open boundary condition for 33 rivers. Flow rate data imposed is based on a combination of daily observations from PREVIMER, simulated data from E-HYPE hydrological model and monthly climatological data from GRDC and French "Banque Hydro" dataset. Further details can be found in Sotillo et al., (2015).

Originally, the operational IBI system was based on a periodic re-initialization from the GLOBAL parent solution. Afterwards, IBI has steadily evolved: by April 2016, an upgrade of the downscaling methodology was implemented, substituting the periodic re-initialization by an spectral nudging technique in order to avoid temporal discontinuity inherent to the periodic re-initialization and minimize dependency from the GLOBAL parent solution on the shelf. The chosen spectral nudging method permits to ″nudge″ the low frequency IBI system solution towards the large scale GLOBAL solution in those areas where this global solution is supposed to be better (mainly off the shelf and in deep waters) due to the assimilation of lower frequency signals. Thus, the nudging is regionally limited in those areas where the parent system can not improve the regional model (e.g. where there is no data assimilation of altimetry or where the physics is missing, for instance on the shelf) or where the spatial filtering processes are potentially damage (for instance close to the bottom or the open boundaries). This spatial weight function is a 3D mask showing transitions between zones where the IBI system is kept nudged (typically off shore, outside from the shelf area, and off the open boundaries) and the ones where IBI remains free. Finally, a SAM2-based data assimilation scheme (Lellouche et al., 2013; Brasseur et al., 2005) was recently introduced (April 2018) in order to enhance IBI predictive skills but will not be further described here as only outputs from 2017 have been used in the present work.

3.3 PdE SAMPA coastal system

The PdE-SAMPA operational forecast service started in April 2012 (Sammartino et al., 2014; Sánchez-Garrido et al., 2014). It routinely provides a daily short-term forecast (72-h horizon) of currents and other oceanographic variables in the Gibraltar Strait and its surroundings (Gulf of Cadiz and Alboran Sea). The PdE-SAMPA model application was developed by the University of Malaga in collaboration with PdE and it is based on the Massachusetts Institute of Technology global circulation model -MITgcm- (Marshall et al., 1997). The domain, which extends from the Gulf of Cádiz to the Alboran Sea, is discretized with an orthonormal curvilinear grid of variable horizontal resolution, sparser close to the boundaries (~ 8-10 km) and higher in GIBST (~ 300-500 m). In the vertical dimension, SAMPA has 46 unevenly spaced z levels with maximum resolution of 5 m near the surface, exponentially decaying towards the seafloor. The shallower level is at 2.5 m depth. The bathymetry is derived from a combination of the GEBCO bathymetry data set and fine-resolution bathymetric charts of the Strait of Gibraltar and the continental shelf of the Gulf of Cadiz and northern coast of the Alboran Sea. The bottom topography is represented as partial vertical cells. In the two lateral open boundaries (west and east) the model is forced by daily mean temperature, salinity and velocity fields from CMEMS-IBI regional model (Sotillo et al., 2015). In addition, tidal and meteorologically-driven barotropic velocities are prescribed across the open boundaries, the former extracted from the model described by Carrere and Lyard (2003) and the latter from the storm surge operational system developed by Álvarez-Fanjul et al. (2001), which accounts for the remote effect of the atmospheric forcing in the barotropic flow through GIBST. At the sea surface, the model is forced by hourly values of wind stress, air humidity and temperature, fresh water and heat surface fluxes provided by the Spanish Meteorological Agency through the operational Forecast System based on the HIRLAM model (Cats, G.; Wolters, 1996). Further details on the SAMPA model configuration are provided in Sanchez-Garrido et al. (2013).

4 Validation of OOFSs

4.1 Framework

The validation of OOFSs against independent measurements constitutes a core activity in oceanographic operational centres since it aids: i) to infer the relative strengths and weaknesses in the modelling of several key physical processes; ii) to compare different versions of the same OOFS and evaluate potential improvements and degradations before a new version is transitioned into operational status; iii) to compare coarse resolution 'father' and nested high-resolution 'son' systems to quantify the added value of downscaling.

With regards to the third aspect, IBI forecast products are regularly intercompared not only against other CMEMS regional model solutions (e.g. NWS and MED) in the overlapping areas (Lorente et al., 2017) but also against its parent system (GLOBAL) by means of NARVAL (North Atlantic Regional VALidation) login-protected web-based application (Sotillo et al. 2015). This tool has been implemented to routinely monitor IBI performance and to objectively inter-compare models' reliability and prognostic capabilities. Both real-time validation ('online mode') and regular-scheduled 'delayed-mode' validation (for longer time periods) are performed using a wealth of observational sources as benchmark, among others: in situ observations from buoys and tide-gauges, SST satellite derived products, temperature and salinity profiles from ARGO floats and HFR. Product quality indicators and skill metrics are automatically computed in order to infer IBI accuracy and the spatiotemporal uncertainty levels. The evaluation metrics regularly generated by NARVAL are online delivered in the QUID, which is periodically updated and freely available in CMEMS website (http://marine.copernicus.eu/).

Complementarily, opportunistic inter-comparisons are conducted in the frame of diverse EU-funded projects such as MEDESS-4MS (Sotillo et al., 2016-a): 35 satellite tracked drifters were released on both sides of the Strait of Gibraltar and the quality-controlled in situ data of sea surface temperature and currents were collected to build the MEDESS-GIB database (Sotillo et al., 2016-b), providing hence a complete Lagrangian view of the surface inflow of Atlantic waters through the GIBST and the Alboran Sea. Such valuable oceanographic information was subsequently used to intercompare IBI and SAMPA forecast products to identify strengths (realistic simulation of the Atlantic Jet and the Algerian Current) and shortcomings (position and intensity of the Alboran gyres, especially the western one) in both models performance. This exercise reflected the effectiveness of the dynamical downscaling performed through the SAMPA system with respect to the regional solution (in which SAMPA is nested), providing an objective measure of the potential added value introduced by SAMPA.

Eventually, ancillary validation approaches have been recently adopted focused on the evaluation of ocean models performance in specific situations and on their ability to accurately reproduce singular oceanographic processes (Hernández et al., 2018). Since the NARVAL tool is devoted to inter-compare model solutions on a monthly, seasonal or annual basis, part of the picture is missing due to traditional time averaging. Hence the quality indicators computed, albeit valid, mask somehow models´ capabilities to replicate ocean phenomena of particular interest at shorter timescales. This event-oriented multi-model inter-comparison methodology allows to better infer the ability of each system to capture small-scale coastal processes. In this context, the recurrent question "*Which model is the best one?*" should be reformulated by firstly admitting that one system can outperform the rest of OOFs for a particular event but by contrast can be also beaten when attempting to reproduce and characterize some other distinct ocean phenomenon.

Those oceanographic events subject of further insight might encompass, among others: i) coastal upwelling, dowelling and relaxation episodes; ii) submesoscales eddies (Mourre et al., 2018); iii) extreme events; iv) complete flow reversals. Particularly, in the present work the attention has been devoted to the full and permanent reversal of the surface AJ in the GIBST during, at least, 48 hours. This unusual episode has been detected by means of HFR current estimations and further examined with OOFSs outcomes. The agreement between both in situ and remote-sensing instruments and the ocean forecasting system has been evaluated by means of computation of a set of statistical metrics traditionally employed in this framework: histograms, bias, root mean squared differences (RMSD), scalar and complex correlation coefficients, current roses, histograms, quantile-quantile (QQ) plots and the best linear fit of scatterplots. In the following sub-section all the in situ and remote-sensed observations employed in the present work are described.

4.2 Observational data sources

In situ observations

The study domain includes an array of buoys operated by Puertos del Estado and the Irish Marine Institute (Figure 1, a), providing quality-controlled hourly-averaged observations of SST, SSS and currents. To ensure the continuity of the data record, occasional gaps detected in time series (not larger than 6 hours) were linearly interpolated. Basic features of each in-situ instrument are described in Table 2.

Satellite-derived observations

The European Ocean Sea Surface Temperature L3 Observations is a CMEMS operational product which provides a daily fusion of SST measurements from multiple satellite sensors over a 0.02° resolution grid. The L3 multi-sensor (supercollated) product is built from bias-corrected L3 mono-sensor (collated) products. If the native collated resolution is N and $N < 0.02$ the change (degradation) of resolution is done by averaging the best quality data. If $N > 0.02$ the collated data are associated to the nearest neighbour without interpolation nor artificial increase of the resolution. A synthesis of the bias-corrected L3 mono-sensor (collated) files remapped at resolution R is done through a selection of data based on the following hierarchy: AVHRR_METOP_B, SEVIRI, VIIRS_NPP, AVHRRL-19, AVHRRL-18, MODIS_A, MODIS_T, AMSR2. This hierarchy can be changed in time depending on the health of each sensor. Further details can be found in the Product User Manual (PUM), freely available in CMEMS website (http://cmems-resources.cls.fr/documents/PUM/CMEMS-SST-PUM-010-009.pdf)

HFR-derived observations

The HFR system employed in the present study consists of three-site shore-based CODAR Seasonde network, installed in GIBST (Fig 1, b-c). Hereafter the sites will be referred to by their four letter site codes: CEUT, CARN, and TARI, respectively (Figure 1, c). Each site is operating at a central frequency of 26.8 MHz, providing hourly radial current measurements which are representative of the upper 0.5 m of the water column. The maximum horizontal range and angular resolution are 40 km and 5º, respectively. Radial current measurements from the three stations are geometrically combined with an averaging radius set to 3 km, in order to estimate hourly total current vectors on a Cartesian regular grid of 1x1 km horizontal resolution.

A source of error to be considered in the computation of the total vectors is the so-called Geometrical Dilution of Precision (GDOP). The GDOP is defined as a dimensionless coefficient of uncertainty that characterizes how radar system geometry may impact on the measurements accuracy and position determination errors, owing to the angle at which radial vectors intersect. Maps of east and north GDOP for this HFR system (not shown) follow a pattern where their values increase with the distance from the radar sites and along the baselines (lines connecting two HFR sites), as the combining radial vectors are increasingly parallel and the orthogonal component tends to zero. Further details can be obtained from Lorente et al. (2018).

The accuracy of HFR measurements, which are affected by intrinsic uncertainties (radio frequency interferences, environmental noise, etc.) have been previously assessed by comparing against in situ observations provided by a point-wise current meter (Lorente et al., 2014), yielding correlations above 0.7 and RMSD below 13 $cm \cdot s^{-1}$. Such results revealed that this HFR network has been operating within tolerance ranges, properly monitoring the surface circulation in near real-time of this geostrategic region.

Recent works relying on this HFR system have successfully investigated the water exchange between Algeciras Bay and the Strait of Gibraltar (Chioua et al., 2017), the impact of the atmospheric pressure fluctuations on the mesoscale water dynamics of the Strait of Gibraltar and the Alboran Sea (Dastis et al., 2018), the dominant modes of spatio-temporal variability of the surface circulation (Soto-Navarro et al., 2016) or the characterization of the Atlantic surface inflow into the Mediterranean Sea (Lorente et al., 2018).

In the present work, quality-controlled hourly HFR current measurements collected during the entire 2017 were used as benchmark to elucidate the skill of a number of OOFSs. As shown in Figure 1-c, the data availability was significantly high: almost 100% in the selected transect, decreasing in the easternmost sectors. The transect here used to examine the AJ surface inflow was readily chosen as the associated total GDOP, reported in Lorente et al (2018), was reduced (below 1.3) and the spatial and temporal data availability were optimal during 2017. From an oceanographic perspective, the election of such transect was also convenient to better characterize both the intensity and direction of the AJ, since its midpoint covers the area where the highest peak of current speed is usually detected and also where the inflow orientation is not influenced yet by the water exchange between Algeciras Bay and the Strait of Gibraltar.

5 Comparison between CMEMS model solutions in IBI waters

Temperature

The CMEMS L3 satellite-derived daily data were used to validate the SST fields predicted by both GLOBAL and IBI. Maps of SST anomalies were computed on a monthly basis (Figure 2). Apparently, both models behaved similarly during winter (defined as JFM). In January, low warm anomalies were detected off-shelf in northwest Atlantic waters, while cold SST anomalies were encountered in coastal areas of the English Channel and the Irish Sea, and also surrounding the Balearic Islands in the Western Mediterranean (Figure 2, a-b). By March, the moderately positive western anomalies migrated southwards within IBI domain

Ocean Sci. Discuss., https://doi.org/10.5194/os-2018-168
Manuscript under review for journal Ocean Sci.
Discussion started: 17 January 2019

(Figure 2, c-d). The negative bias previously observed almost disappeared around the Balearic Islands and in the Irish Sea, turning even into slightly warm anomalies inside the English Channel in the case of GLOBAL.

During spring months (AMJ), a small positive bias spread over almost the entire IBI domain (Figure 2, e-f). In May, GLOBAL outputs exhibited a moderate SST overestimation (around 1ºC) in the English Channel, the Irish Sea and the southern part of the North Sea (Figure 2, e). In addition, a narrow belt of warm SST anomalies could be observed along the African coastal upwelling system (ACUS hereinafter) and over the continental shelf break (evident until late July). An increased vertical mixing during summer has been previously postulated to reduce the SST observed over the continental shelf break with respect to the surrounding ocean (Graham et al., 2018), thus explaining such strip of warm bias. By contrast, since IBI presents a higher grid resolution, it could partially resolve the internal waves breaking which leads to turbulence and energy for increased vertical mixing with cooler waters beneath the pycnoclyne, ultimately contributing to the reduced SST bias observed in IBI estimations over the continental shelf break (Figure 2, f). Besides, IBI properly reproduced the SST field in the northern IBI area although clearly overpredicted coastal temperatures over ACUS, in the periphery of the Canarias Islands.

During summertime (JAS), the warm SST spring anomalies previously identified in both GLOBAL and IBI became even more pronounced in July, locally reaching values up to 2ºC (Figure 2, g-h). Besides, new features were revealed as a result of the onset of the upwelling season, such as the positive bias in the Iberian Upwelling System (IUS), higher in the case of IBI (Figure 2, h). According to the reduced bias in both western coastal upwelling systems (Figure 2, g), GLOBAL seemed to better replicate the SST field likely thanks to recent progresses in data assimilation schemes and to the growing wealth of available observational data. In this context, future data sets (satellite SSS and swath SST) should improve constrains on model behaviour (Gasparin et al., 2018). By September, a portion of the warm anomalies detected in GLOBAL outputs vanished in the Irish Sea and the English Channel although a dipole of positive-negative anomalies could be clearly observed in the North Sea (Figure 2, i). By contrast, in the case of IBI the SST overestimation expanded over the entire ICANA sub-region (as defined in Figure 1, a) and the Gulf of Lion (Figure 2, j). Furthermore, the summer positive anomaly developed in the Western Alboran Sea became warmer, likely linked to the inadequate representation of the speed and direction of the Atlantic Jet, something that will be addressed in the following sections.

By the end of the year (Figure 2, k-l), both models appeared to better fit to observations as reflected by the smoothed SST anomalies in northern (southern) sub-regions observed for GLOBAL (IBI). GLOBAL underestimated again the SST over the Irish Sea and the English Channel (Figure 2, k) as it previously did in January (Figure 2, a), thus closing the cold-warm-cold anomalies cycle during 2017. The alternation between winter cold anomalies and summer warm anomalies were earlier identified by Graham et al. (2018) and related to a possible over-stratification in coastal regions. With regards to IBI predictions, a relevant cold bias was detected in the Western Mediterranean, particularly over the Algerian Current and the Almeria-Oran Front (Figure 2, l).

It is worth mentioning that availability of satellite observations is lower close to the shorelines and the associated intrinsic uncertainties are higher, probably due to the impact of the land mask on the optimal interpolation process conducted to transform the original satellite tracks into a regular grid, justifying to some extent the predominance of SST anomalies in coastal areas.

Complementary skill metrics, spatially-averaged over the entire IBI service (IBISR) domain, were depicted on a monthly basis (Figure 3, a). While significantly high correlation coefficients (above 0.95) remained rather constant for both OOFS, monthly RMSD exhibited a marked seasonal cycle with lower values in winter (0.4ºC), a spring rise reaching a peak of 0.7ºC by July due to the aforementioned model SST overestimation, followed by a steady decay during the last part of the year. GLOBAL performance was more accurate from July to December as indicated by the lower RMSD.

According to the sub-regional monthly statistics (Figure 3, b-j), a rather similar sequence could be also found for open-water zones such us the Gulf of Biscay (GOBIS, Figure 3-b) or the Western Mediterranean (WSMED, Figure 3-c): permanently consistent correlations (above 0.8) and higher RMSD for the second part of the year. In other sub-regions, the RMSD evolved in like fashion while summer correlation values decreased down to [0.4-0.6] ºC: Gulf of Cadiz (CADIZ, Figure 3-d), Canarias Islands (ICANA, Figure 3-i) and Strait of Gibraltar (GIBST, Figure 3, j). In near-coast areas, skill metrics fluctuated differently: in the Western Iberian Shelf (WIBSH, Figure 3-e), higher RMSD were observed in winter and summer as a consequence of a likely misrepresentation of the freshwater discharge during the rainy season and of the coastal upwelling under northerly wind regime, respectively. By contrast, in the Northern Iberian Shelf (NIBSH, Figure 3-f) the monthly correlation coefficient oscillated without a clear pattern, ranging from 0.4 (March and December) to 0.8 (early summer). Furthermore, IBI seemed to outperform GLOBAL in the two northernmost sectors within the study-domain: English Channel (ECHAN, Figure 3-g) and Irish Sea (IRISH, Figure 3-h) in terms of higher correlation and lower RMSD, especially pronounced during summertime. Tidally driven mixing could account for a portion of the discrepancies encountered between the coarser detided GLOBAL and IBI model solutions, where the former predicts an over-stratification in shelf-seas. Finally, as SST estimations are routinely assimilated in GLOBAL system, a more precise performance is generally expected offshore, as proved for ICANA or WESMED, among other sub-regions.

Results above exposed reveal that SST divergences between IBI and GLOBAL forecast datasets are mainly found on the shelf near coastal areas featuring a complex bathymetry. For the sake of completeness, supplementary validation works in the entire 3D water column with Argo-floats are regularly conducted to assess model vertical structure (not shown, we refer the reader to the QUID). Both models perform fairly well in open-waters, given the fact that GLOBAL assimilates this type of in situ observations and subsequently transfers the information to the nested IBI system thanks to the aforementioned spectral nudging technique. Nevertheless, validation focused on smaller scales and high frequency processes is still crucial to analyse in detail the performance of both modelled products in intricate coastal regions.

Hourly in situ observations from eight buoys, moored within specific sub-regions (Figure 1, a), were used as benchmark to validate both GLOBAL and IBI outputs. The annual time series of SST exhibited a significantly high resemblance, properly reproducing the expected annual-cycle shape (Figure 4). According to the consistent skill metrics derived from the comparison against three deep-water buoys (B3, B4 and B5, in Table 2), both models had a rather alike performance during 2017 with RMSD and correlation coefficients in the ranges [0.44-0.96] ºC and [0.86-0.99], respectively (Figure 4: c, d, e). While the similar behaviour observed off the shelf is partially attributable to the aforementioned spectral nudging technique, the model-observation comparison in near-shore areas revealed noticeable discrepancies.

Ocean Sci. Discuss., https://doi.org/10.5194/os-2018-168
Manuscript under review for journal Ocean Sci.
Discussion started: 17 January 2019

Ocean Science Discussions

On one hand, IBI appeared to outperform GLOBAL system in the Irish Sea (Figure 4, b), Gulf of Cadiz (Figure 4, f) and GISBT sub-region (Figure 4, g), as reflected by lower (higher) RMSD (correlation) values obtained. Particularly, the results for the Strait of Gibraltar are not in complete accordance with the statistics previously derived from the comparison against L3 satellite-derived data (Figure 3, j), likely due to the fact that remote-sensed SST estimations area might be affected by higher intrinsic uncertainties (i.e. land contamination and cloud cover). Although both comparisons against remote and in situ observations confirmed the model SST overestimation in GIBST, especially during summertime, the former (latter) indicated that IBI precision was significantly lower (higher). Another relevant aspect is the notable ability of IBI to capture sharp summer SST drops (steeper than 3ºC) during prevalent easterlies (Figure 4, g), as a result of the surface inflow reversal and subsequent intrusion of warmer Mediterranean waters into GIBST (this phenomenon will be subject of further analysis in Section 7). However, GLOBAL appeared to overestimate SST in this area during the entire year, as reflected by a RMSD of 1.64ºC.

On the other hand, GLOBAL seemed to behave slightly better at B1 location -IBISR area- (Figure 4, a) and substantially more accurately at B8 buoy location - in the Canarias Islands, ICANA-, where a permanent SST overestimation from June to December was evidenced in IBI predictions (Figure 4, h), yielding thereby a RMSD twice higher than that obtained for GLOBAL estimations, in agreement with Figure 2 (i-j) and Figure 3 (i). The lower performance of IBI in ICANA sub-region was previously reported by Aznar et al (2016) when inter-comparing IBI forecast and 1/12º reanalysed solutions. At this point it is worth recalling that GLOBAL includes a data assimilation scheme, whereas IBI takes realistic ocean conditions from weekly global analyses. This fact shows up the possible benefits of the observational data assimilation in these areas, at least in terms of surface variables. Furthermore, a fraction of observed model-buoy discrepancies in SST can be explained in terms of disparate depth scales: whereas IBI and GLOBAL daily outputs are representative of the temperature in the upper one meter of the water column, moored buoys provide temperature estimations at a deeper nominal depth (between 1 and 3.5 m, depending on the brand).

Complementarily, a quarterly analysis was performed to infer any potential degradation in model performances during a specific season of the year (Figure 5). Overall, both GLOBAL and IBI predictions seemed to be more reliable in winter (except at B1 location: Figure 5-a) in terms of lower RMSD. They also emerged to be less realistic during summer, as denoted by abrupt decreases in quarterly correlation indexes (from 0.9 down to 0.5) at B2, B4 and B6 locations and the relevant rise of RMSD (up to 2.5ºC) at B7 location (GIBST sub-region). This SST overestimation could be partially explained in terms of imprecise latent sensible heat fluxes and excess of evaporation, although additional efforts should be devoted to shed light on it. Once again, IBI performance appeared to be more accurate in coastal zones featuring a more complex bathymetry (at B2, B4, B6 and B7 locations), whereas GLOBAL fitted better to in situ observations in off shelf regions such as at B1 and B8 locations. In the rest of the cases, both model solutions were rather alike. It is noteworthy that each point-wise buoy is not representative of the entire sub-region in which is deployed, explaining thus to some extent the discrepancies arisen between sub-sections 6.1 and 6.2.

Salinity

As pointed out in the introduction, the enhancement of riverine forcing is still as a priority in ocean modelling as the estuarine circulation is mainly driven by horizontal density gradients which are ultimately modulated by freshwater inputs. In this context, previous

Ocean Sci. Discuss., https://doi.org/10.5194/os-2018-168
Manuscript under review for journal Ocean Sci.
Discussion started: 17 January 2019

works have investigated the potential benefits of replacing old climatologies by data from hydrological model predictions (O´Dea et al., 2017). Here we provide a specific example to illustrate the discrepancies between GLOBAL and IBI performances in the Galician coast (NW Spain), as a consequence of the different horizontal resolution and distinct runoff forcing implemented in the operational chain. While both models performances are rather similar in open-waters (according to the results derived from the validation against 3D Argo-float profiles and exposed in the QUID), higher discrepancies are expected to arise in coastal and shelf areas as they are governed by small-scale processes such as land-sea breezes, runoff (and the resulting stratification and buoyancy-driven circulation), transport materials (nutrients, sediments, pollutants, etc.).

As shown in Figure 6-a, hourly in situ SSS data collected by B4 buoy during March 2018 experienced an abrupt decrease from a standard value around 36 PSU down to almost 33 PSU in just few hours during the 20th of March, likely due to a noticeable filament of freshwater discharged by Miño River. IBI outputs at the closest grid point appeared to properly capture both the sharp drop in SSS values and the persistent low salinity values for the next 4-day period. By the end of the month, the modelled salinity field seemed to steadily recover to usual levels in the range of 35.5-35.8 PSU, whereas in situ observations revealed a steeper rise to 34.8 PSU by the 23th of March. Nevertheless, the skill metrics confirmed the accurate IBI performance, with a correlation coefficient of 0.92 and a RMSD of 0.33 PSU. By contrast, although GLOBAL outputs could replicate the mean SSS, it did not reproduce satisfactorily the freshwater episode and barely showed any temporal variability, as reflected by a negligible correlation coefficient (0.09) and a higher RMSD (0.84 PSU).

Consequently, the impact of colder freshwater river inputs on the SST was also evaluated (Figure 6, b). Once again, while the sudden cooling of 1.5ºC denoted by in situ observations was fairly well replicated by IBI, GLOBAL system could only correctly predict the overall decreasing trend along with the SST values immediately before (13.5ºC) and after (13ºC) the analysed event. As a consequence, the monthly correlation coefficient (RMSD) obtained for IBI is higher (lower): 0.79 versus 0.20 (0.25ºC versus 0.35ºC).

The buoyancy input introduced by large freshwaters fluxes (particularly during the spring freshet), together with topographic effects, contributed to the development of the well-documented Western Iberian Buoyant Plume (Peliz et al., 2002; Otero et al., 2008), which strongly influenced the shelf circulation, forming an averaged veering to ∼270º (measured clockwise from the North) during 20th-21st of March, as reflected by in situ observations and IBI outputs (Figure 6, c). However, GLOBAL could only partially reproduce the prevailing surface flow as modelled currents were mainly advected to the south-southwest (180º-270º). Equally, IBI appeared to correctly replicate the acceleration of the upper-layer stream from 10 to 45 $cm \cdot s^{-1}$ due to impulsive-type freshwater river outflow already observed in situ estimations of sea surface currents (Figure 6, d). Notwithstanding, GLOBAL current intensity remained moderated (below 20 $cm \cdot s^{-1}$) during most part of March, including the selected episode, as reflected by the poorer skill metrics obtained. The current speed underestimation observed in this tidal environment is mainly attributable to the fact that GLOBAL system provides a detided solution, so barotropic tidal velocities do not contribute to the final prescribed total velocity.

Daily-averaged maps of modelled SSS and SST were computed for the 21st of March (Figure 6, e-h) to infer the differences between GLOBAL and IBI. As it can be seen, the former showed a relatively-smoothed and spatially-homogeneous decrease in the salinity and temperature fields along the entire coastline (Figure 6, e-f), while the latter exhibited more intricate patterns with many filaments together with a significant drop in SSS and SST (Figure 6, g-h) in the periphery of the three main local rivers mouth (from North to South: Miño, Douro and Tagus) as a result of freshwater plumes flowing out over saltier Atlantic waters. In this three cases, the SST field could effectively act as a tracer for the salinity stratification.

There is a significant resemblance between the monthly current roses derived from in situ observations and IBI predictions in terms of speed and mean direction (Figure 6, i), showing the predominance of the so-called Iberian Poleward Current, flowing northwards and circuiting the western and northern Iberian margins under prevailing southerly winds (Torres and Barton, 2006). GLOBAL current outputs differed from observations, exhibiting an overall tendency for eastward directions. The skill metrics derived from time series comparison at B4 buoy location confirmed that the regional OOFS outperformed the global one during March 2018, hence postulating the benefits of improved horizontal resolution to better resolve the plume dynamics and its extension off-shelf. In addition, the increased horizontal resolution of IBI allows to better resolving individual frontal fluctuations and horizontal salinity gradients by preserving the signal of river plume narrower, closer to the coast and with a more complex structure. The impact of model resolution in both the horizontal extent of the plume and the strength and position of the freshwater front has been subject of previous studies (Bricheno et al., 2014). Since both models present 50 depth levels and similar vertical discretization, the horizontal resolution and the riverine forcing are assumed to play a primary role when attempting to explain the differences encountered in models performance for this specific test-case.

6 Circulation in the Strait of Gibraltar: multi-model inter-comparison from global to coastal scales

Proved the relevance of the intensity and orientation of the AJ in determining the surface circulation of the Alboran Sea, the ability of each OOFS to portray the upper layer circulation in the GIBST area has been evaluated. The annually-averaged surface pattern provided by the HFR network revealed north-eastward speeds around 100 $cm \cdot s^{-1}$ in the narrowest section of the Strait (Figure 7, a). SAMPA coastal model seemed to capture well the time-averaged intensity and orientation of the Atlantic inflow (Figure 7, b), whereas IBI regional model clearly overestimated the mean surface circulation speed (Figure 7, c). Finally, the coarser OOFS (GLOBAL) barely captured the most basic features on the incoming flow and its subsequent propagation towards the north-east (Figure 7, d).

As this qualitative model-intercomparison on a yearly basis was insufficient to infer the skilfulness of each system, a quantitative validation at the midpoint of the selected transect (Figure 1, c) was assessed. The scatter plot of HFR-derived hourly current speed versus direction (taking as reference the North and positive angles clockwise) revealed interesting details (Figure 8, a): firstly, the AJ flowed predominantly eastwards, forming an angle of 78º respect the North. The current velocity, on average, was 100 $cm \cdot s^{-1}$ and reached peaks of 250 $cm \cdot s^{-1}$. Speeds below 50 $cm \cdot s^{-1}$ were registered along the entire range of directions. Westwards currents, albeit minority, were also observed and tended to predominantly form an angle of 270º.

The scatter plot of SAMPA estimations presented a significant resemblance in terms of prevailing current velocity and direction (Figure 8, b). Although the time-averaged speed and angle were slightly smaller (90 $cm \cdot s^{-1}$) and greater (88º), respectively, the main features of the AJ were qualitatively reproduced: maximum velocities (up to 250 $cm \cdot s^{-1}$) were associated with an eastward flow and an AJ orientation in the range of 50º - 80º. Besides, surface flow reversals to the west were properly captured.

By contrast, noticeable differences emerged in the scatter plot of regional IBI estimations (Figure 8, c): surface current velocities below 30 cm·s^{-1} were barely replicated and the AJ inversion was only observed very occasionally. Despite the fact that IBI appeared to properly portray the mean characteristics of the eastwards flow, the model tended to privilege flow directions comprised between 60º and 180º and to overestimate the current velocity, with averaged and maximum speeds around 117 cm·s^{-1} and 280 cm·s^{-1}, respectively.

In the case of the scatter plot derived from GLOBAL estimations, even more substantial discrepancies were detected as the variability of both the AJ direction and speed were clearly limited to the range 65º-80º and 50-200 cm·s^{-1}, respectively (Figure 8, d). No flow reversals were detected and peak velocities of the eastward flow were underestimated.

The scatter plots of observation-model differences provided relevant information (Figure 8, e-g). In the case of SAMPA, discrepancies were clustered around zero for both parameters, with an asymptotic distribution along the main axes (Figure 8, e). On the contrary, a negative bias to negative differences as observed for both IBI (Figure 8, f) and GLOBAL (Figure 8, g), especially for the latter. In other words, the regional and global OOFSs overestimated both the current speed and the angle of the AJ, reflecting a tendency to more south-easterly directions (clockwise rotated respect the north). Overall, a steady improvement in the AJ characterization is evidenced in model performance when zooming from global to coastal configurations, highlighting the benefits of the dynamical downscaling approach.

Additional statistical indicators were computed: two histograms illustrated the number of hourly zonal (U) and meridional (V) velocity data per class interval (Figure 9, a-b). HFR-derived zonal velocity estimations exhibited a Gaussian-like shape clustered around 84 cm·s^{-1} and slightly shifted to lower values in the case of SAMPA coastal model (79 cm·s^{-1}). Both datasets show similar positive bias and variability, with the standard deviation around 56-57 cm·s^{-1} for 2017 (Figure 9, a). IBI and GLOBAL presented narrowed histograms, with distributions positively biased and constrained to zonal velocities above 0 and 40 cm·s^{-1}, respectively. In the case of meridional currents, each distribution exhibits a nearly symmetrical Gaussian-like shape but biased towards different values (Figure 9, b). Whilst SAMPA and its parent system IBI exhibited an alike distribution (and moderately similar to that revealed for HFR estimations), GLOBAL histogram emerged again dramatically shortened and restricted only to positive values, revealing a recurrent predominance of the AJ to flow north-eastwards.

Based on the QQ-plot for the zonal velocity component (Figure 9, c), it can be concluded that SAMPA estimations were consistent despite the slight overestimation observed for the highest velocities (95th–100th percentiles). The general IBI overestimation along the entire range of percentiles was also clearly evidenced. In accordance with its histogram, GLOBAL system overestimated (underestimated) zonal currents below (above) the 90th percentile. A similar behaviour was also observed for GLOBAL meridional velocities, this time around the 20th percentile (Figure 9, d). On the contrary, both SAMPA and IBI appeared to generally underestimate the meridional surface current speed, even more for higher percentiles.

Class-2 skill metrics, gathered in Table 3, were also computed in order to provide a quantitative perspective of models performance at the midpoint of the selected transect. SAMPA clearly outperformed both parent systems, as reflected by lower RMSD values for both velocity components together with a complex correlation coefficient (CCC) and phase (CCP) of 0.79 and -8º, respectively, which means that SAMPA predictions were highly correlated with HFR current observations although slightly clockwise rotated (i.e., more south-eastwards). The agreement between HFR hourly data and IBI and GLOBAL estimations, albeit significant (CCC above 0.6), was lower as the related phase values decreased substantially (especially for GLOBAL: CCP below -20º), indicating a more zonal surface flow.

The three systems predicted more precisely the zonal velocity component than the meridional one, with scalar correlations emerging in the ranges [0.68-0.83] and [0.15-0.56], respectively. Notwithstanding, RMSD were more moderate for the latter (below 37 $cm \cdot s^{-1}$) than for the former (below 53 $cm \cdot s^{-1}$). This could be attributed to the extremely intense and predominant West-East zonal exchange of Atlantic-Mediterranean waters through GIBST, with the meridional flow playing a residual role.

The statistical results derived from SAMPA-HFR comparison, gathered in Table 3, are in line with those earlier obtained in a 20-month validation performed by Soto-Navarro et al. (2016), which reported correlations of 0.70 and 0.27 for the zonal and meridional velocities, respectively. The observed model-radar discrepancies might be attributed to the fact that the uppermost z-level of SAMPA model is 2.5 m, while HFR observations are representative of the first 0.5 m of the water column and thus more sensitive to wind forcing. This might explain some model drawbacks detected in relation to the reduced energy content in surface current speeds, as reflected by the positive bias between HFR estimations and SAMPA outputs (Table 3)

Complementarily, the multi-model inter-comparison exercise in the GIBST region focused on the ability to adequately reproduce an extreme event: the quasi-permanent full reversal of the AJ surface flow during, at least, 48 hours when intense easterlies episodes were prevalent. Under this premise, only four episodes were detected and categorized during the entire 2017 (Figure 10). The prevailing synoptic conditions were inferred from ECMWF predictions of sea level pressure (SLP: Figure 10, a-d) and zonal wind at 10 m height (U-10: Figure 10, e-h). A significant latitudinal gradient of SLP was observed in 3 episodes (February, March and December), with high pressures over the Gulf of Biscay and isobars closely spaced in GIBST, giving rise to very strong easterlies (above 10 $m \cdot s^{-1}$), channelled through the Strait (Figure 10: e, f and h). In August, the typical summer weather type was observed with Azores High pressures governing the Atlantic Area and moderate but persistent easterly winds blowing through the entire Western Mediterranean (Figure 10: c, g).

Both atmospheric variables were spatially-averaged over specific sub-regions (WSMED and GIBST, respectively, indicated by a red square in Figure 10: a-h) and 3-hourly monitored along the selected months (Figure 10: i-p). Very high SLP values and extremely high (negative) U-10 (i.e., intense easterlies) led to a complete inversion of the surface flow, from the prevailing eastward direction to a westward outflow into the Atlantic Ocean, as reflected in the Hovmöller diagrams computed for the HFR-derived zonal currents (Figure 10, q-t). In February, a brief 24-h inversion (related to less intense easterlies) preceded the full reversal of the surface flow (Figure 10, q). Likewise, the event detected in March consisted of an abrupt interruption and complete reversal of the eastwards AJ (Figure 10, r). By contrast, in August and December, the classical AJ inflow into the Mediterranean was only observed in the southern part of the transect, whereas a weaker coastal counter current was detected flowing westwards and bordering the Spanish shoreline (Figure 10, s-t). Such coastal flow inversion has been previously reported and subject to further analysis by Reyes et al. (2015). Particularly, the flow reversal detected in August was not triggered by high SLP (Figure 10, k) but induced by moderate and persistent easterlies (5 $m \cdot s^{-1}$, Figure 10-o).

Ocean Sci. Discuss., https://doi.org/10.5194/os-2018-168
Manuscript under review for journal Ocean Sci.
Discussion started: 17 January 2019

Short-lived reversals of the surface inflow have been previously reported to occur almost every tidal cycle in Camarinal Sill (western end of GIBST: Figure 1-b) mainly due to the contribution of the semidiurnal tidal component M_2 (Reyes, 2015; Sannino, et al. 2004; García Lafuente, et al., 1990; La Violette and Lacombe 1988). Since the mean inflow of Atlantic water is modulated by barotropic tidal currents, hourly-averaged sea surface height (SSH) observations provided by Tarifa tide-gauge (Figure 1, c) were used to elucidate if the four 2-day inflow reversal events in the eastern end of the Strait could have been mostly influenced by spring-neap tidal cycle fluctuations (Figure 10, u-x). Although the fortnightly variability was clearly observable in a monthly time series of SSH, no cause-effect relationship could be visually inferred from the inspection of zonal velocities at the selected transect (Figure 10, q-t). Apparently, evidence of preference for a specific tidal cycle was not observed as the four flow reversal episodes took place under strong easterlies but during different tidal conditions, ranging from neap tides (Figure 10, u) to spring tides (Figure 10: v, x). As shown in Lorente et al. (2018), tides seemed to play a secondary role by partially speeding up or slowing down the westward currents, depending on the phase of the tide. These results are in accordance with previous modelling studies (Sannino et al., 2004) where the contribution of the semidiurnal tidal component to the transport was proved to be relevant over the Camarinal Sill, (incrementing the mean transport by about 30%, for both the inflow and the outflow), whereas it was almost negligible at the eastern end of the Strait.

The observed 2-day averaged HFR-derived circulation patterns associated with the four events here studied were depicted in Figure 11 (a, e, i, m). Some common peculiarities were exposed, such as the overall westward outflow through the narrowest section of GIBST or the subtle anticyclonic inflow into the Algeciras Bay. Three study cases revealed a predominant circulation towards the West together with a marked acceleration of the flow in the periphery of Algeciras Bay, reaching speeds above 70 cm·s^{-1} (Figure 11: a, e, i). The fourth case (December 2017) was substantially less energetic and exhibited a rather counter-clockwise recirculation in the entrance to GIBST. (Figure 11, m). On the other hand, two episodes illustrated how the circulation in the easternmost region of the study domain followed a clockwise rotation (Figure 11: e, m).

From a qualitative perspective, SAMPA was able to reproduce fairly well at least two of the four inversion episodes in terms of overall circulation pattern in GIBST and adjacent waters (Figure 11: f, j, n). In the event of March, SAMPA replicated the intense eastern anticyclonic gyre, with velocities up to 80 cm·s^{-1}, along with the inflow into the Algeciras Bay. However, the model could only partially resolve the AJ inversion, exhibiting a counter-clockwise recirculation with the outflow restricted to the north-western Spanish shoreline (Figure 11, f). In the episode corresponding to 4th–5th of December (Figure 11, n), the upper-layer dynamic was rather similar to the previously described for March, albeit less vigorous. The visual resemblance with HFR map (Figure 11, m) was generally high, according to common features observed: the eastern anticyclonic gyre, the central belt of currents circulating towards the North-West and eventually the cyclonic recirculation structure in the entrance to GIBST. On the contrary, in the event occurred between 14th-15th of August (Figure 11, j), a moderate observation-model resemblance was deduced in the northeastern sector of the domain: SAMPA was able to resolve the observed southwestward stream, the inflow into the Algeciras Bay and the weak intrusion of Mediterranean waters into GIBST bordering the northern shoreline but, by contrast, it was ultimately impelled to join the general AJ inflow governing the Strait and propagating towards the east. Finally, although SAMPA predicted the occurrence AJ reversal by 20th–21st of February (Figure 11, b), the simulated circulation structure partially differed from that observed with HFR estimations (Figure 11, a). Whereas the formed prognosticated a meander-like circulation, a predominant cross-shore stream within the channel and a flow inversion uniquely circumscribed to the entrance of GIBST, the latter provided an overall westward outflow from the Mediterranean Sea into the Atlantic Ocean.

In the case of IBI, the Atlantic inflow was always present. In two episodes, the intense AJ was directed towards the North-East (Figure 11: g, o), converging with the overall clock-wise gyre that dominated the easternmost region, which was already observed in HFR estimations (Figure 11: e, m). By contrast, in the two remaining episodes the surface inflow was predominantly zonal (Figure 11, c) and directed south-eastwards (Figure 11, k), respectively. Whereas in the former event no common features could be observed between the HFR and IBI, in the latter a moderate observation-model resemblance was deduced in the northeastern sector of the domain, as similarly occurred with SAMPA estimations (Figure 11, j). Leaving aside the counter-clockwise eddy observed in IBI pattern (Figure 11, k), absent from HFR map (Figure 11, i), IBI partially resolved the observed southwestward flow, the circulation into the Algeciras Bay and the westward penetration of surface waters along the northern shoreline of the Strait. Finally, GLOBAL system barely replicated the HFR-derived circulation patterns as the northeastward stream was permanently locked, showing further reduced speed variations from one episode to another (Figure 11: d, h, l, p).

Among the physical implications of the surface inflow reversal, abrupt increases in the SST field were revealed, especially during summertime when warmer surface waters outflowed into the Atlantic from the Mediterranean (Figure 12). During August 2017, the aforementioned CCC raised the day 11th and lasted until the end of the month, confined at higher latitudes except for the already analysed 2-day event of 14th-15th, coinciding with the full reversal mentioned (Figure 12, a). The monthly inter-comparison of the zonal currents at the midpoint of the selected transect (represented by a black square in Figure 12-a) confirmed the progressive improvement of the multi-nesting strategy, according to the skill metrics obtained (Figure 12, b). SAMPA and IBI were able to accurately reproduce the wide tidal oscillations, although only the former could properly capture the flow inversions represented by negative zonal velocities that took place between the 14th-15th and between 21st-24th of August. GLOBAL detided outputs only reproduced basic features of the surface flow, showing always smoothed eastward velocities. As a consequence, skill metrics for the coastal OOFS were better than for its parent system, and recursively regional skill metrics were in turn better than global ones, in terms of higher (lower) correlation (RMSD) values. Analysis for the meridional velocity component (not shown) revealed similar results, with the SAMPA outperforming the coarser models. Notwithstanding, the three OOFS proved to be more skilled to forecast zonal than meridional currents. The complex correlation coefficient and the related phase were 0.85 and -7.37º, respectively, indicating both the relevant SAMPA-HFR agreement and the slight veering of model outputs respect HFR estimations: a negative value denoted a clockwise rotation of modelled current vectors (i.e., a more southwardly direction). In the case of IBI, although the phase was similar (-7.92º) the complex correlation was lower (0.72). GLOBAL current vectors were, on average, significantly veered clockwise (-25.71º), despite the high complex correlation coefficient (0.70).

From the 11th of August, a progressive warming of 7.5ºC at the upper ocean layer of the northern shoreline was observed (Figure 12, c), according to the in situ estimations provided by B7 buoy (whose latitude is located with a solid black dot in Figure 12-a). As easterly winds progressively dominated the study-area and persisted enough, the CCC broadened and the complete inflow reversal transported warmer Mediterranean waters to the west through the entire transect, as reflected by the pronounced SST maximum (~25ºC) detected soon afterwards, by the 18th of August. A secondary peak of SST was monitored by the 25th, before the CCC started weakening. In accordance with previous statements about model behaviour for the zonal currents, once again SAMPA outperformed the parent systems as reflected by a significantly high correlation of 0.89 and a lower but statistically relevant RMSD of 1.22ºC. IBI presented a general bias (positive the first week of august and negative the rest of the month) but adequately reproduced the temporal variability of the SST field (correlation of 0.67). In the case of GLOBAL, the system could not benefit from data assimilation in this intricate coastal area with low level of available observations: worse skill metrics were subsequently obtained, with a correlation of 0.65 and a RMSD above 2ºC.

Finally, outputs from SAMPA high-resolution coastal model were used to provide further insight into the entire AJ-WAG system and how diversity from the classical picture of the Alboran Sea surface circulation emerged from changes in the intensity and direction of the AJ. Although only one episode (corresponding to December 2017) is here shown (Figure 13), the four events followed a similar scenario:

i) *Prelude*: the classical AJ was observed flowing vigorously (with velocities clearly above 80 $cm \cdot s^{-1}$) northeastwards into the Alboran Sea and feeding the WAG (Figure 13, a-b).

ii) *Onset*: as westerly wind lost strength, the AJ speed became progressively weaker and the jet tended to flow more southwardly, giving rise to a weakening and subsequent decoupling of the AJ-WAG system along with the genesis of a new small-scale coastal eddy that coexisted with the WAG (Figure 13, c-d). Circulation snapshots with three gyres (including the EAG, out of the pictures) have been previously reported in the literature (Flexas et al., 2006; Viúdez et al., 1998). The new eddy could be either cyclonic and confined northeast of Algeciras Bay (February 2017, not shown) or anticyclonic and starting to detach from the coast and migrate eastwards (Figure 13, e-f). Meanwhile, the WAG presented different configurations: from an almost-symmetric aspect (August 2017, not shown) to a more elongated shape in the cross-shore direction (December 2017: Figure 13-f) or in the along-shore direction (March 2017, not shown).

iii) *Development*: The AJ velocity reached a minimum (below 50 $cm \cdot s^{-1}$) associated with a sharp change in the predominant wind regime from westerlies to easterlies (Figure 13, g-h). A branch of the eddy, neighboring the Strait, was wind-weakened and deflected from the main rotating pathway and started to flow westwards to the GIBST.

iv) *Full establishment of the inflow reversal*: complete westward outflow from the Mediterranean Sea into the Atlantic Ocean through the narrowest section of GIBST, reaching a peak of velocity over Camarinal Sill (Figure 13, i). The migratory eddy and the WAG started merging into one single anticyclonic gyre (Figure 13, j).

v) *Epilogue*: Afterwards, in three of the cases the re-settlement of predominant westerlies (Figure 10: m, n, p) favoured the return of the northeastward oriented Atlantic inflow and the consequent reactivation of the usual AJ-WAG system (not shown). By contrast, in the fourth episode (August 2017), summer easterly winds kept blowing moderately for two extra weeks (Figure 10, o) but were too weak to preserve the induced reversal, thus the Atlantic inflow reappeared again.

7 Conclusions

The current generation of ocean models have undergone meticulous tuning based on several decades of experience. The ever-increasing inventory of operational ocean forecasting

Ocean Sci. Discuss., https://doi.org/10.5194/os-2018-168
Manuscript under review for journal Ocean Sci.
Discussion started: 17 January 2019

systems provides the society with a significant wealth of valuable information for high-stakes decision-making and coastal management. Some of them are routinely operated on overlapping regions, offering the opportunity to compare them, judge the strengths and weaknesses of each system and eventually evaluate the added-value of high-resolution coastal models respect to coarser parent model solutions.

In this work, a multi-parameter model inter-comparison was conducted at the sea surface, ranging from global to local scales in a two-phase strategy. Firstly, a comparison of CMEMS products (GLOBAL and the nested IBI regional system) was performed against remote-sensed and in situ observations. In terms of temperature, results highlighted the overall benefits of both the GLOBAL data assimilation in open-waters and the increased horizontal resolution of IBI in coastal areas, respectively. IBI outperformed its coarser parent system in those coastal regions characterized by a jagged coastline and a substantial slope bathymetry. As GLOBAL has a smoothed bathymetry and do not resolve many narrow features of the real sea floor, the depths where mixing takes place could be biased. Besides, those mixing processes acting at scales smaller than the grid cell size might substantially affect the resolved large-scale flow in the coarser GLOBAL system.

On the other hand, since GLOBAL is a detided model solution, tidally-driven mixing could account for a portion of the discrepancies found between GLOBAL and satellite-derived SST estimations in energetic tidal areas such as the English Channel, the North Sea and the Irish Sea. Whereas GLOBAL seemed to predict an over-stratification in shelf-seas, IBI could better reproduce the vertical stratification and hence the SST field in the aforementioned subregions.

Complementarily, an isolated but rather illustrative example of the impact of impulsive-type river freshwater discharge on local surface circulation in NW Spain was provided. The increased horizontal resolution of IBI allowed a more accurate representation of horizontal salinity gradients, the horizontal extent of the plume and the strength and position of the freshwater front, according to the results derived from the validation against in situ observations of SSS, SST and currents provided by a moored buoy. Since both GLOBAL and IBI present 50 depth levels, similar vertical discretization and comparable climatological runoff forcing, the horizontal resolution is assumed to play a primary role when attempting to explain the differences encountered in models performance for this specific test-case. Notwithstanding, the authors are fully aware of this single isolated example does not suffice and additional events over the entire IBI coastal domain should be examined in future works.

Finally, a 1-year (2017) multi-model inter-comparison exercise was performed in the Strait of Gibraltar between GLOBAL, IBI and the nested SAMPA coastal system in order to elucidate the accuracy of each OOFS to characterize the AJ dynamic. A quantitative comparison against hourly HFR estimations highlighted both the steady improvement in AJ representation when moving from global to coastal scales though a multi-nesting model approach and also the relevance of a variety of factors at local scales, among others:

i) A sufficiently detailed representation of bathymetric features: the very high horizontal resolution of SAMPA (~ 400 m) and, consequently, the tailored bathymetry employed in order to capture small-scale ocean process and resolve sharp topographic details.

ii) A better representation of air-sea interactions: the adequate refinement of the spatio-temporal resolution of the atmospheric forcing used in SAMPA, especially in a complex coastal region where topographical steering further impacts on flows.

iii) The inclusion of accurate tidal and meteorologically-driven barotropic velocities, prescribed across the open boundaries, allowed a detailed examination of persistent

Atlantic inflow reversal episodes. Although the matching between HFR observations and SAMPA outputs is mainly found in two of the four reversal events detected, this result demonstrates its added value as modelling tool towards the comprehension of such singular oceanographic event. A detailed characterization of this phenomenon is relevant from diverse aspects, encompassing search and rescue operations (to adequately expand westwards the search area), the management of accidental marine pollution episodes (to establish alternative contingency plans), or safe ship routing (to maximize fuel efficiency).

Finally, SAMPA coastal model outputs were analysed in order to put in a broader perspective the context of the onset, development and end of such flow reversal and its impact on the AJ-WAG coupled system. The synergistic approach based on the integration of HFR observing network and SAMPA predictive model has proved to be valid to comprehensively characterize the highly dynamic coastal circulation in the GIBST and the aforementioned episodic full reversals of the surface inflow. In this context, data assimilation would provide the integrative framework for maximizing the joint utility of HFR-derived observations and coastal circulation models. A data assimilation scheme could be incorporated in future operational versions of SAMPA in order to improve its predictive skills, since similar initiatives are currently ongoing with positive results (Hernández-Lasheras et al., 2018; Vandenbulcke et al., 2017; Stanev et al., 2015).

Future efforts are planned to improve CMEMS global and regional OOFSs in several aspects already addressed in the present work. While GLOBAL system will be evolved towards a 1/36º model application, a substantial refinement will be accomplished for regional IBI system in both vertical and horizontal resolutions: from 50 to 75 depth layers and from 1/36º to 1/108º (~1 km), respectively. Whereas the first feature will be incorporated during CMEMS Phase-2 (2018-2021), the second milestone will be achieved in the frame of Inmerse H2020 project and is expected to positively impact on a more accurate representation of coastal processes, among others: submesoscale shelf break exchanges and connectivity, fronts, river plumes or topographic controls on circulation.

In addition, a more detailed bathymetry is expected to be introduced in future operational versions of IBI in order to better resolve those regions with complex coastline and intricate bottom topography. Other factors that could be potentially improved but still deserve further analysis are the air-sea and the land-sea interactions, i.e., the meteorological and riverine forcings. With regards to the former, a more skilful atmospheric forecast model with a higher spatiotemporal resolution (i.e., hourly prediction over a more refined grid) could aid to better represent the coastal circulation by a more accurate discrimination of the topographic structures and the replication of the inertial oscillations and mesoscale processes. On the other hand, each main river basin hydrology should be more accurately represented with daily-updated outputs from tailored hydrological models. Finally, refined mixing schemes might also produce notable improvement in the representation of water masses, resulting in a substantial reduction of temperature and salinity bias relative to model solution.

References

Álvarez-Fanjul, E., Pérez, B. and Rodríguez, B.: A description of the tides in the Eastern North Atlantic, Progress in Oceanography, 40, 217–244, 1997.

Álvarez-Fanjul., E., Pérez, B. and Rodríguez, I.: Nivmar: a storm surge forecasting system for Spanish waters, Sci. Mar., 65, 145-154, 2001.

Álvarez-Fanjul et al.: Operational Oceanograhy at the Service of the Ports. In "New Frontiers in Operational Oceanography". E. Chassignet, A. Pascual, J. Tintoré and J. Verron, Eds., GODAE OceanView, 729-736, doi:10.17125/gov2018.ch27, 2018.

Aznar, R., Sotillo, M.G., Cailleau, S., Lorente P., Levier, B., Amo-Baladrón, A., Reffray, G. and Álvarez-Fanjul, E.: Strengths and weaknesses of the Copernicus forecasted and reanalyzed solutions for the Iberia-Biscay-Ireland (IBI) waters, Journal of Marine Systems, 159, 1-14, 2016.

Brasseur, P., Bahurel, P., Bertino, L., Birol, F., Brankart, J.M., Ferry, N., Losa, S., Remy, E., Schröter, J., Skachko, S., Testut, C.-E., Tranchant, B., Van Leeuwen, P.J. and Verron, J.: Data assimilation for marine monitoring and prediction: the MERCATOR operational assimilation systems and the MERSEA developments, Q. J. R., Meteorol. Soc, 131, 3561-3582, doi: 10.1256/qj.05.142, 2005.

Bricheno, L.M, Wolf, J.M. and Brown, J.M.: Impacts of high resolution model downscaling in coastal regions, Continental Shelf Research, 87, 7-16, 2014.

Caldeira, R., Couvelard, X., Vieira, R., Lucas, C., Sala, I. and Vallés Casanova, I.: Challenges on building an operational forecasting system for small island regions: regional to local, Journal of Operational Oceanography, 9, 1-12, 2016.

Carrere, L. and Lyard, F.: Modelling the barotropic response of the global ocean to atmospheric wind and pressure forcing – comparisons with observations, Geophys. Res. Lett., 30 (6), 1-8, 2003.

Cats, G. and Wolters, L.: The Hirlam project, International Journal of Computational Science and Engineering, 3, 4-7, 1996.

Chioua, J., Dastis, C., Gonzalez, C.J., Reyes, E., Mañanes, R., Ruiz, M.I., Álvarez-Fanjul, E., Yanguas, F., Romero, J., Álvarez, O. and Bruno, M.: Water exchange between Algeciras Bay and the Strait of Gibraltar: a study based on HF coastal radar, Estuarine Coastal and Shelf science, 196, 109-122. doi: 10.1016/j.ecss.2017.06.030, 2017.

Cotelo, C., Amo-Baladrón, A., Aznar, R, Lorente, P., Rey, P. and Rodriguez, A.: On the successful coexistence of oceanographic operational services with other computational workloads, International Journal of High Performance Computing Applications, 1-12, doi: 10.1177/1094342017692045, 2017.

Dai, A., Qian, T., Trenberth, K. and Milliman, J.D.: Changes in continental freshwater discharge from 1948 to 2004, J. Climate, 22, 2773-2792, 2009.

Dastis, C., Izquierdo, A., Bruno, M., Reyes, E., Sofina, E.V. and Plink, N.L.: Influence of the atmospheric pressure fluctuations over the Mediterranean Sea on the mesoscale water dynamics of the Strait of Gibraltar and the Alboran Sea, Fundamentalnaya i Prikladnaya Gidrofisika, 11 (1), 28-29, doi: 10.7868/S2073667318010033, 2018.

Dorman, C.E., Beardsley, R.C. and Limeburner, R.: Winds in the Strait of Gibraltar, Q.J. Meteorol. Soc., 121, 1903-1921, 1995.

Egbert, G.D. and Erofeeva, S.Y.: Efficient inverse modeling of barotropic ocean tides, Journal of Atmospheric and Oceanic Technology, 19, 183–204, 2002.

Federico, I., Pinardi, N., Coppini, G., Oddo, P., Lecci, R. and Mossa, M.: Coastal ocean forecasting with an unstructured grid model in the southern Adriatic and northern Ionian seas, Nat. Hazards Earth Syst. Sci., 17, 45-59, 2017.

Flexas, M., Gomis, D., Ruiz, S., Pascual, A. and Leon, P.: In situ and satellite observations of the eastward migration of the Western Alboran Sea Gyre, Prog. Oceanogr., 70, 486-509, 2006.

García-Lafuente, J., Almazán, J.L., Fernández, F., Khribeche, A. and Hakimi, A.: Sea level in the Strait of Gibraltar: Tides, Int. Hydrogr. Rev., LXVII, 111–130, 1990.

García-Lafuente, J., Delgado, J. and Criado, F.: Inflow interruption by meteorological forcing in the Strait of Gibraltar, Geophysical Research Letters, 29 (19), 1914, 2002.

García-Lafuente, J., Álvarez-Fanjul, E., Vargas, J.M. and Ratsimandresy, A.W.: Subinertial variability in the flow through the Strait of Gibraltar, J. Geophys. Res.: Oceans, 107 (C10), 3168, doi:10.1029/2001JC001104, 2002.

Gasparin, F., Greiner, E., Lellouche, J.M., Legalloudec, O., Garric, G., Drillet, Y., Bourdallé-Badie, R., Le Traon, P.Y., Rémy, E. and Drévillon, M.: A large-scale view of oceanic variability from 2007 to 2015 in the global high resolution monitoring and forecasting system at Mercator Ocean, Journal of Marine Systems, 2018 (in press).

Graham et al.: AMM15: a new high-resolution NEMO configuration for operational simulation of the European North-West shelf, Geosci. Model Dev., 11, 681-696, 2018.

Greenberg, D.A., Dupont, F., Lyard, F.H., Lynch, D.R. and Werner, F.E.: Resolution issues in numerical models of oceanic and coastal circulation, Continental Shelf Research 27, 1317-1343, 2007.

Grifoll, M., Jordá, G., Sotillo, M.G., Ferrer, L., Espino, M., Sánchez-Arcilla, A. and Álvarez-Fanjul, E.: Water circulation forecasting in Spanish harbours. Scientia Marina, 76, S1, 45-61, doi: 10.3989/scimar.03606.18B, 2012.

Herbert, G., Garreau, P., Garnier, V., Dumas, F., Cailleau, S., Chanut, J., Levier, B., and Aznar, R.: Downscaling from oceanic global circulation model towards regional and coastal model using spectral nudging techniques: application to the Mediterranean Sea and IBI area models, Mercator Ocean Quarterly Newsletters, 49, 44, April 2014.

Hernández, F. et al.: Measuring performances, skill and accuracy in operational oceanography: New challenges and approaches. In “New Frontiers in Operational Oceanography“. E. Chassignet, A. Pascual, J. Tintoré and J. Verron, Eds., GODAE OceanView, 759-796, doi:10.17125/gov2018.ch29, 2018.

Hlevca, B., Wells, M.G., Cruz Font, L., Doka, S.E., Portiss, R., John, M.S. and Cooke, S.J.: Water circulation in Toronto Harbour, Aquatic Ecosystems Health and Management, doi: 10.1080/14634988.2018.1500059, 2018.

Holt, J., Hyder, P., Ashworth, M., Harle, J., Hewitt, H.T., Liu, H., New, A.L., Pickles, S., Porter, A., Popova, E., Allen, J.I., Siddorn, J. and Wood, R.: Prospects for improving the representation of coastal and shelf seas in global ocean models, Geosciences Model Development, 10, 499-523, 2017.

Ocean Sci. Discuss., https://doi.org/10.5194/os-2018-168
Manuscript under review for journal Ocean Sci.
Discussion started: 17 January 2019

Katavouta, A. and Thompson K.R. Downscalling ocean conditions with application to the Gulf of Maine, Scotian shelf and adjacent deep ocean, Ocean Modelling, 104, 54-72, 2016.

Kourafalou, V.H., De Mey, P., Staneva, J., Ayoub, N., Barth, A., Chao, Y., Cirano, M., Fiechter, J., Herzfeld, M., Kurapov, A., moore, A.M., Oddo, P., Pullen, J., Van der Westhuysen, A. and Weisberg, R.: Coastal Ocean Forecasting: science drivers and user benefits, Journal of Operational Oceanography, 8 (1), Special Issue: GODAE Oceanview part 1, 147-167, doi:10.1080/1755876X.2015.1022348, 2015.

Large, W.G. and Yeager, S.G.: Diurnal to decadal global forcing for ocean and sea-ice models: the data sets and flux climatologies, NCAR technical notes, 2004.

Hernández-Lasheras, J., Mourre, B., Reyes, E., Orfila, J., Juza, M., Aguiar, E. and Tintore, J.: Assimilating Ibiza Channel HF radar currents in a high resolution model, Geophysical Research Abstracts, 20, EGU General Assembly, Vienna, April 2018.

La Violette, P.E. and Lacombe, H.: Tidal-induced pulses in the flow through the Strait of Gibraltar, In Oceanol. Acta, Special Issue 0399-1784, Océanographie Pélagique Méditerranéenne, Villefranche-sur-Mer, France, Minas, H.J., Nival, P., Eds., 13–27, 1988.

Lellouche, J.-M., Greiner, E., Le Galloudec O, Garric G., Regnier C., Drevillon M., Benkiran M., Testut C.E., Bourdalle-Badie R., Gasparin, F., Hernández O, Levier B., Drillet Y., Remy E. and Le Traon P.Y.: Recent updates to the Copernicus marine Service global ocean monitoring and forecasting real-time 1/12º high resolution system, Ocean Science, 14, 1093-1126, 2018.

Lellouche, J.-M., Le Galloudec, O., Drévillon, M., Régnier, C., Greiner, E., Garric, G., Ferry, N., Desportes, C., Testut, C.-E, Bricaud, C., Bourdallé-Badie, R., Tranchant, B., Benkiran, M., Drillet, Y., Daudin, A. and De Nicola, C.: Evaluation of global monitoring and forecasting systems at Mercator Océan, Ocean Sci., 9, 57-81, 2013.

Le Traon, P.Y. et al.: The Copernicus Marine Environmental Monitoring Service: Main Scientific Achievements and Future Prospects, Mercator Ocean Journal, 56, CMEMS Special Issue, 2018.

Lin, J.G., Chiu, Y.F. and Weng W.K.: Wave forecast system of Hualien Harbour. In: Taiwan-Polish Joint Seminar on Coastal Protection, 37-46, 2008.

Lorente, P., Piedracoba, S., Soto-Navarro, J. and Álvarez-Fanjul, E.: Accuracy assessment of High Frequency radar current measurements in the Strait of Gibraltar, Journal of Operational Oceanography, 7 (2), 59–73, 2014.

Lorente, P., Sotillo M.G., Dabrowski T., Amo-Baladrón, A., Aznar R., Pascual, A., Levier, B., Bowyer, P., Cossarini, G., Salon, G., Tonani, M. and Álvarez-Fanjul, E.: Intercomparison of different operational oceanographic forecast products in the CMEMS IBI area, Poster at the European Geosciences Union (EGU), Vienna, Austria, April 2017.

Lorente, P., Piedracoba, S., M.G. Sotillo, and Álvarez-Fanjul, E.: Long-term monitoring of the Atlantic Jet through the Strait of Gibraltar with HF radar observations, Journal of Marine Science and Technology, 6, 1-16, 2018.

Lyard, F., Lefevre, F., Letellier, T. and Francis, O.: Modelling the global ocean tides: modern insights from FES2004, Ocean Dynamics, 56, 394-415, 2006.

Macias, D., García-Gorriz, E. and Stips, A.: The seasonal cycle of the Atlantic Jet dynamics in the Alboran sea: direct atmospheric forcing versus Mediterranean thermohaline circulation, Ocean Dynamics, 66, 137-151, doi: 10.1007/s10236-015-0914-y, 2016.

Macías, D., Martín, A.P., García-Lafuente, J., García, C.M., Yool, A., Bruno, M., Vázquez-Escobar, A., Izquierdo, A., Sein, D.V. and Echevarría, F.: Analysis of mixing and biogeochemical effects induced by tides on the Atlantic-Mediterranean flow in the Strait of Gibraltar through a physical-biological coupled model, Prog. Oceanogr., 74 (2-3), 252-272, doi: 10.1016/j.pocean.2007.04.006, 2007a.

Macías, D., Navarro, G., Echevarría, F., Garcia C.M. and Cueto, J.L.: Phytoplankton pigment distribution in the North-Western Alboran Sea and meteorological forcing: a remote sensing study, J. Mar. Res, 65, 523-543, 2007b.

Macías, D., Bruno, M., Echevarría, F., Vázquez, A. and Garcia C.M.: Meteorologically-induced mesoscale variability of the North-Western Alboran sea (southern Spain) and related biological patterns, Estuar Coast Shelf Sci, 78, 250-266, 2008.

Madec G.: NEMO Ocean General Circulation Model, Reference Manual, Internal Report. LODYC/IPSL, Paris, 2008.

Marshall, J., Hill, C., Perelman, L. and Adcroft, A.: Hydrostatic, quasi-hydrostatic, and nonhydrostatic ocean modeling, J. Geophys. Res., 102 (C3), 5733–5752, 1997.

Mourre et al.: Assessment of high-resolution regional ocean prediction systems using multi-platform observations: Illustrations in the Western Mediterranean Sea. In “New Frontiers in operational Oceanography“. E. Chassignet, A. Pascual, J. Tintoré and J. Verron, Eds., GODAE OceanView, 663-694, doi:10.17125/gov2018.ch24, 2018.

O´Dea et al.: The CO5 configuration of the 7 km Atlantic margin model: large-scale biases and sensitivity to forcing, physics options and vertical resolution, Geosci. Model Dev., 10, 2947-2969, 2017.

Otero, P., Ruiz-Villareal, M. and Peliz, A.: Variability of river plumes off Northwest Iberia in response to wind events, Journal of Marine Systems, 72, 238-255, 2008.

Peliz, A., Rosa, T., Santos, A.M.P. and Pisarra, J.: Fronts, jets and counter flows in the Western Iberian upwelling system, Journal of Marine Systems, 35 (1-2), 61-77, 2002.

Pérez, B., Álvarez-Fanjul, E, Pérez, S., de Alfonso, M. and Vela, J.: Use of tide-gauge data in Operational Oceanography, 6 (2), 1-18, 2013.

Pérez, B., Brouwer, R., Beckers, J., Paradis, D., Balseiro, C., Lyons, K., Cure, M., Sotillo, M.G., Hackett, B., Verlaan, M. and Fanjul, E.: ENSURF: multi-model sea level forecast: implementation and validation results for the IBIROOS and Western Mediterranean regions, Ocean Sci. 8 (2), 211–226, 2012.

Pingree, R. and Le Cann, B.: Three anticyclonic slope water eddies (swoddies) in the southern bay of Biscay in 1990, Deep Sea Res, Part A, 39, 1147–1175, 1992.

Reyes, E.: A high-resolution modeling study of the ocean response to wind forcing within the Strait of Gibraltar, Phd. Dissertation, University of Cadiz, Spain, 2015.

Rockel, B.: The regional downscalling approach: a brief history and recent advances, Curr Clim Change Rep, 1, 22-29, doi: 10.1007/s40641-014-0001-3, 2015.

Ruiz, J., Macias, D., Rincón, M., Pascual, A., Catalan, I.A. and Navarro, G.: Recruiting at the edge: kinetic energy inhibits anchovy populations in the Western Mediterranean, Plos One 8 (2), e55523, doi: 10.1371/journal.pone.0055523, 2013.

Sánchez-Arcilla, A., Sierra, J.P., Brown, S., Casas-Prat, M., Nicholls, R.J., Lionello, P. and Conte, D.: A review of potential physical impacts on harbours in the Mediterranean Sea under climate change, Regional Environmental Change, 16, 2471-2484, 2016.

Sánchez-Garrido, J.C., García-Lafuente, J., Álvarez-Fanjul, E., Sotillo, M.G. and De los Santos F.J.: What does cause the collapse of the Western Alboran Gyre? Results of an operational ocean circulation system, Progress in Oceanogrography, 116, 142–153, 2013.

Sánchez-Garrido, J.C., García-Lafuente, J., Sammartino, S., Naranjo, C., De los Santos, F.J. and Álvarez-Fanjul, E.: Meteorologically-driven circulation and flushing times of the Bay of Algeciras, Strait of Gibraltar, Marine Pollution Bulletin, 80, 97-106, 2014.

Sánchez-Garrido, J.C., Naranjo, C., Macías, D., García-Lafuente, J. and Oguz T.: Modeling the impact of tidal flows on the biological productivity of the Alboran Sea, J. Geophys. Res: Oceans, 120, 7329-7345, 2015.

Sannino, G., Bargagli, A. and Artale, V.: Numerical modeling of the semidiurnal tidal exchange through the Strait of Gibraltar, J. Geophys. Res., 109, C05011, doi:10.1029/2003JC002057, 2004.

Sammartino, S., García-Lafuente, J., Sánchez-Garrido, J.C., De los Santos, F.J., Álvarez-Fanjul, E., Naranjo, C., Bruno, M. and Calero-Quesada, C.: A numerical model analysis of the tidal flows in the Bay of Algeciras, Strait of Gibraltar, Continental Shelf Research, 72, 34–46, doi:10.1016/j.csr.2013.11.002, 2014.

Sammartino, S., Sánchez Garrido, J.C., Naranjo, C., García-Lafuente, J., Rodríguez Rubio, P. and Sotillo, M.G.: Water renewal in semi-enclosed basins: A high resolution Lagrangian approach with application to the Bay of Algeciras, Strait of Gibraltar, Limnol. Oceanogr. Methods, 16, 106-118, doi:10.1002/lom3.10231, 2018.

Simpson, J.H.: Physical processes in the ROFI regime, Journal of Marine Systems, 12 (1), 3-15, 1997.

Solé, J., Ballabrera-Poy, J., Macias, D. and Catalán, I.A.: The role of ocean velocity in chlorophyll variability, a modelling study in the Alboran Sea, Scientia Marina, 80 (S1), 249-256, 2016.

Sotillo, M.G., Cailleau, S., Lorente, P., Levier, B., Aznar, R., Reffray, G., Amo-Baladrón, A. and Álvarez-Fanjul, E.: The MyOcean IBI Ocean Forecast and Reanalysis Systems: Operational products and roadmap to the future Copernicus Service, Journal of Operational Oceanography, 8 (1), 1-18, 2015.

Sotillo M.G., Amo-Baladrón, A., Padorno, E., García-Ladona, E., Orfila, A., Rodríguez-Rubio, P., Conte, D., Jiménez J.A., De los Santos, F.J. and Álvarez-Fanjul, E.: How is the surface Atlantic water inflow through the Strait of Gibraltar forecasted? A lagrangian validation of operational oceanographic services in the Alboran Sea and Western Mediterranean, Deep Sea Research, 133, 100-117, 2016-a.

Sotillo M.G., García-Ladona, E., Orfila, A., Rodríguez-Rubio, P., Maraver J.C., Conti, D., Padorno, E., Jiménez J.A., Capó, E., Pérez, F., Sayol, J.M., De los Santos, F.J., Amo-Baladrón, A., Rietz, A., Troupin, C., Tintoré, J. and Álvarez-Fanjul, E.: The MEDESS.GIB database: tracking the Atlantic water inflow, Earth Syst. Sci. Data, 8, 141-149, 2016-b.

Sotillo, M.G., Cerralbo, P., Lorente, P., Grifoll, M., Espino, M. Sánchez-Ercilla, A. and Álvarez-Fanjul, E.: Coastal ocean forecasting in Spanish Ports: the SAMOA operational service, Journal of Operational Oceanography (under review).

Soto-Navarro, J., Lorente, P., Álvarez-Fanjul, E., Sánchez-Garrido, J.C. and García-Lafuente, J.: Surface circulation at the Strait of Gibraltar: a combined HF radar and high resolution model study, Journal of Geophysical Research, Oceans, 121, doi:10.1002/2015jc011354, 2016.

Stanev, E.V., Ziemer, F., Schultz-Stellenfleth, J., Seemann, J., Staneva, J. and Gurgel, K.W.: Blending Surface Currents from HF Radar Observations and Numerical Modelling: Tidal Hindcasts and Forecasts, Journal of Atmospheric and Oceanic Technology, 32, 256-281, 2015.

Stanev, E.V., Schulz-Stellenfleth, J., Staneva, J., Grayek, S., Grashorn, S., Behrens, A., Koch, W. and Pein, J.: Ocean forecasting for the German Bight: from regional to coastal scales, Ocean Science, 12, 1105-1136, doi: 10.5194/os-12-1105-2016, 2016.

Vandenbulcke, L., Beckers, J.M. and Barth, A.: Correction of inertial oscillations by assimilation of HF radar data in a model of the Ligurian Sea, Ocean Dynamics, 67, 117, https://doi.org/10.1007/s10236-016-1012-5, 2017.

Vargas-Yáñez, M., Plaza, F., García-Lafuente, J., Sarhan, T., Vargas, J.M. and Vélez-Belchí, P.: About the seasonal variability of the Alboran Sea circulation, Journal of Marine Systems, 35, 229-248, 2002.

Viúdez, A.: An explanation for the curvature of the Atlantic Jet past the Strait of Gibraltar, Journal of Physical Oceanography, 27, 1804-1810, 1997.

Viúdez, A., Pinot, J.M. and Harney, R.L.: On the upper layer circulation in the Alboran Sea, Journal of Geophysical Research, 103 (C10), 21653-21666, 1998.

Ocean Sci. Discuss., https://doi.org/10.5194/os-2018-168
Manuscript under review for journal Ocean Sci.
Discussion started: 17 January 2019

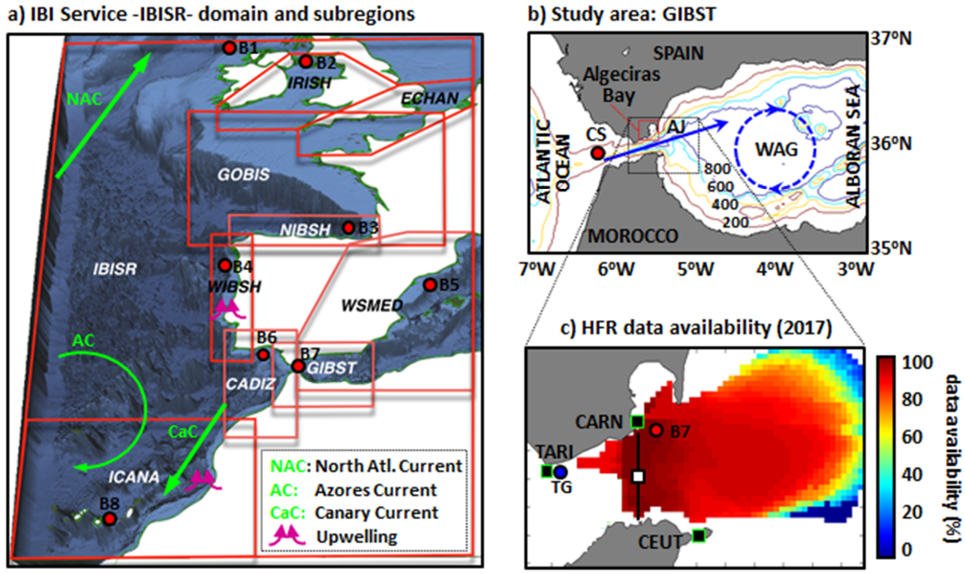

Figure 1. a) Iberia-Biscay-Ireland Service (IBISR) domain, which comprises 9 sub-regions denoted by red squares. Red filled dots represent buoys locations. b) Study area 2: surface Atlantic Jet (AJ) flowing through the Strait of Gibraltar into the Alboran Sea, feeding the Western Alboran Gyre (WAG); isobath depths are labeled every 200 m. Red dot indicates a topographic feature: Camarinal Sill (CS). c) HFR hourly data availability for 2017: solid black squares represent radar sites, blue and red dot indicate Tarifa tide-gauge and B7 buoy location, respectively.

Ocean Sci. Discuss., https://doi.org/10.5194/os-2018-168
Manuscript under review for journal Ocean Sci.
Discussion started: 17 January 2019

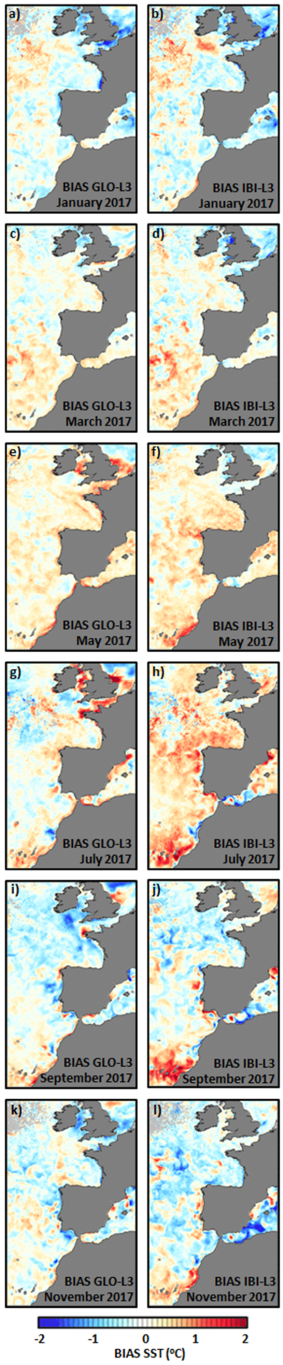

Figure 2. Monthly SST bias (model minus observation), where the satellite-derived daily data used is L3 CMEMS operational product: GLOBAL versus observation (left) and IBI versus observation (right).

Ocean Sci. Discuss., https://doi.org/10.5194/os-2018-168
Manuscript under review for journal Ocean Sci.
Discussion started: 17 January 2019

Ocean Science
Discussions
Open Access

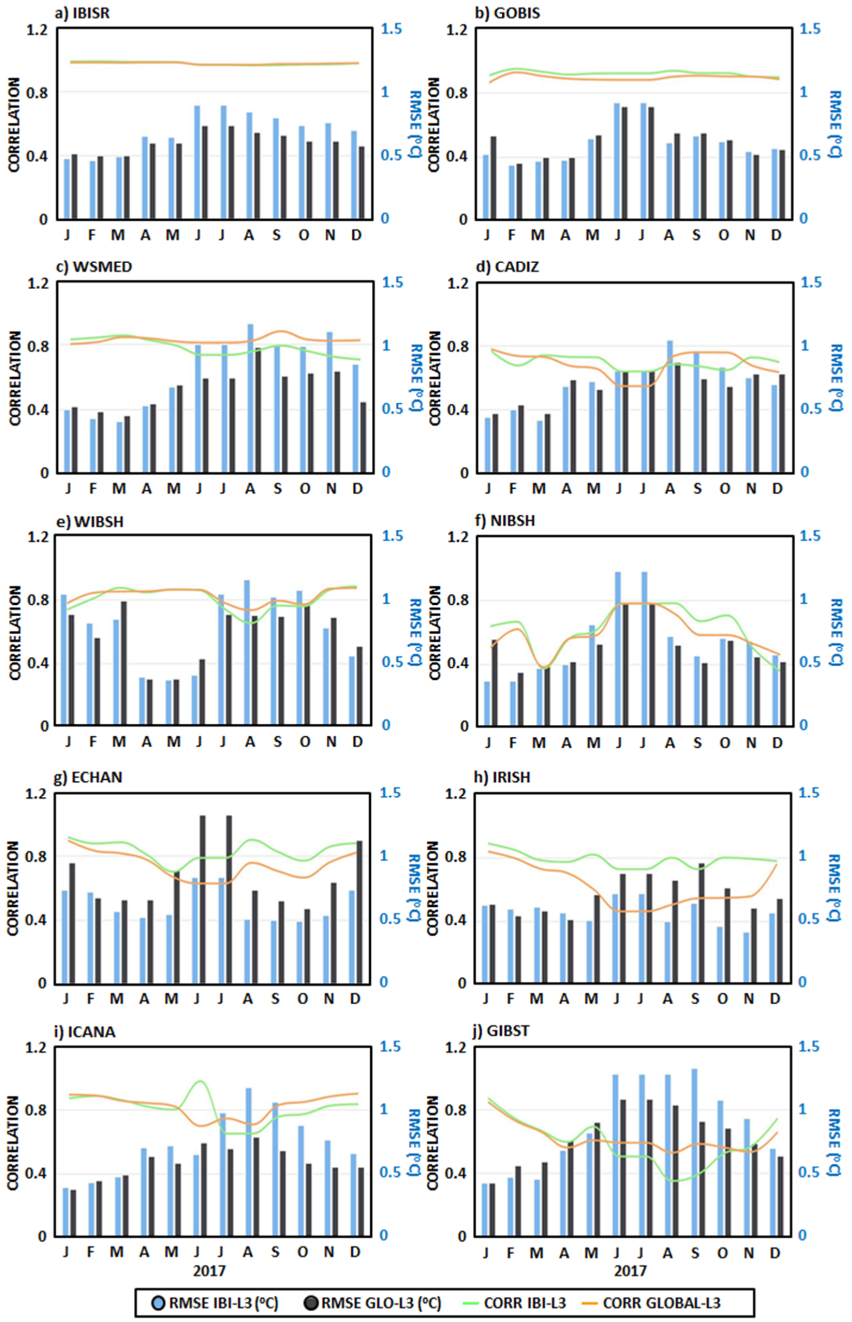

Figure 3. Annual evolution (2017) of monthly skill metrics derived from the comparison of GLOBAL and IBI models against satellite-derived observations (L3) over IBI service domain (IBISR) and nine sub-regions, denoted in Figure 1-a. RMSD values and correlation coefficients are represented by columns and lines, respectively.

Ocean Sci. Discuss., https://doi.org/10.5194/os-2018-168
Manuscript under review for journal Ocean Sci.
Discussion started: 17 January 2019

Ocean Science
Discussions
Open Access

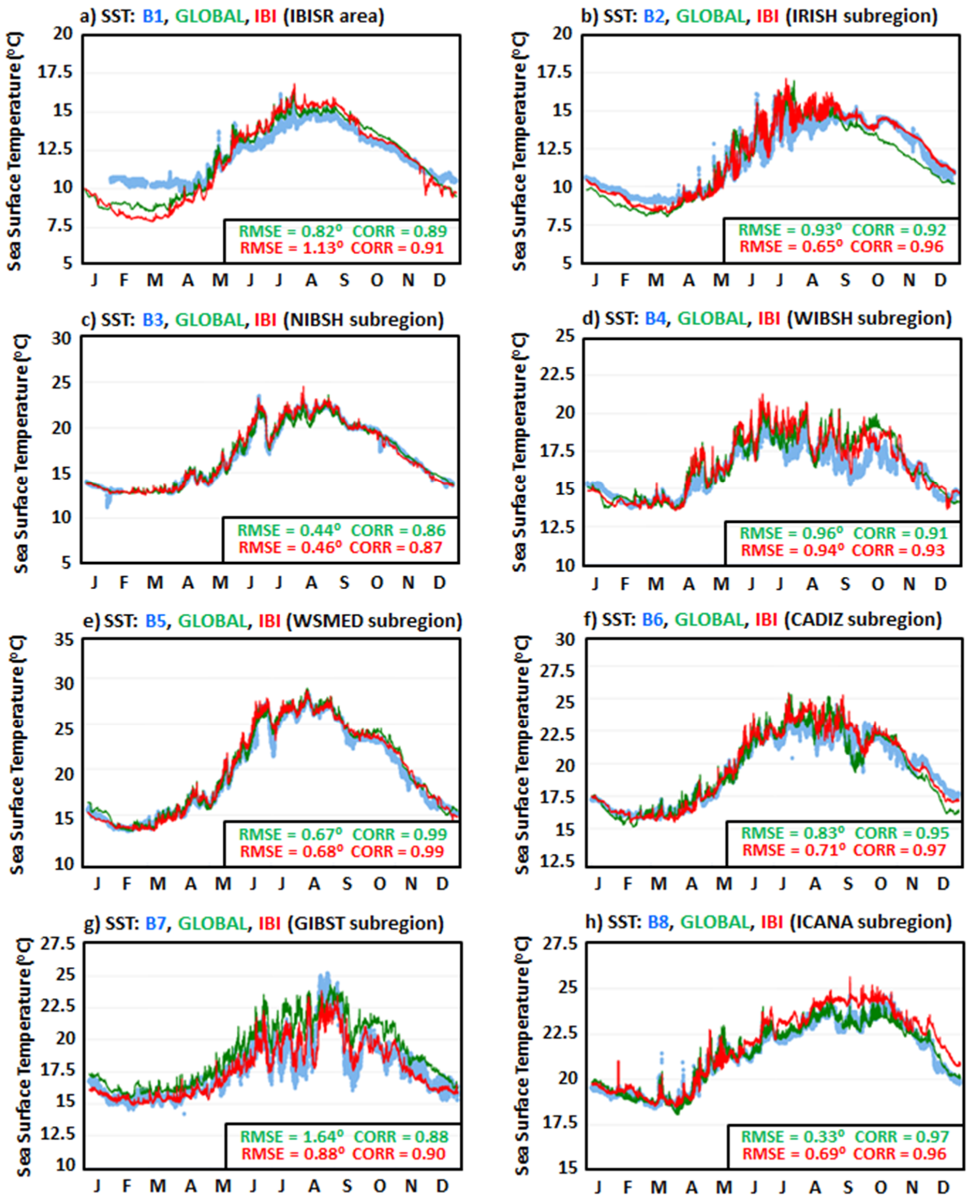

Figure 4. Annual (2017) time series of hourly Sea Surface Temperature (SST) at eight different locations within IBISR area. In situ observations from moored buoys (blue dots), GLOBAL model predictions (green line) and IBI model outputs (red line) are depicted. Skill metrics derived from model-observation comparison are gathered in black boxes.

Ocean Sci. Discuss., https://doi.org/10.5194/os-2018-168
Manuscript under review for journal Ocean Sci.
Discussion started: 17 January 2019

Ocean Science
Discussions
Open Access

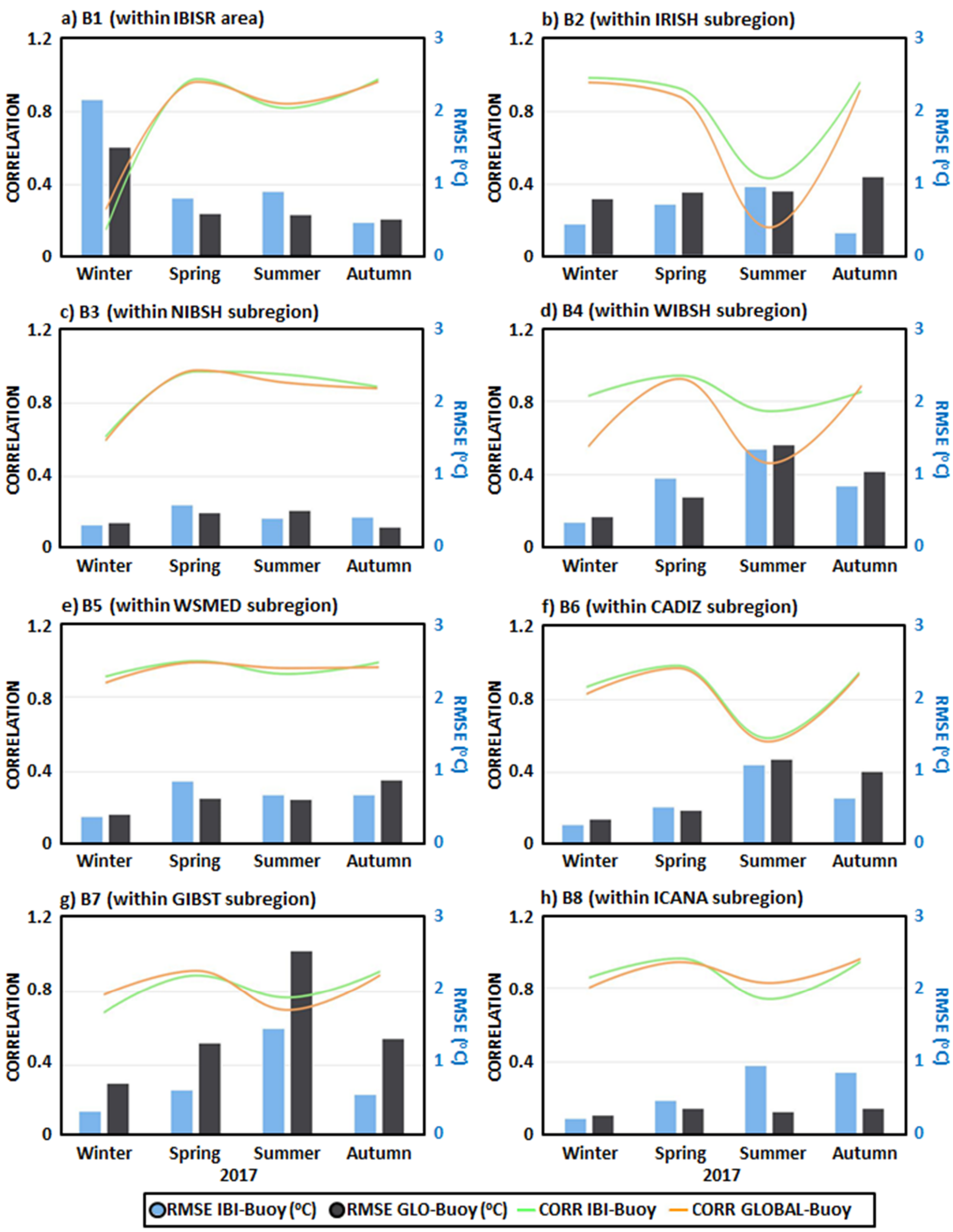

Figure 5. Annual evolution (2017) of seasonal skill metrics derived from the comparison of GLOBAL and IBI models against in situ SST hourly observations provided by eight buoys. RMSD and correlation coefficient represented by coloured bars and lines, respectively.

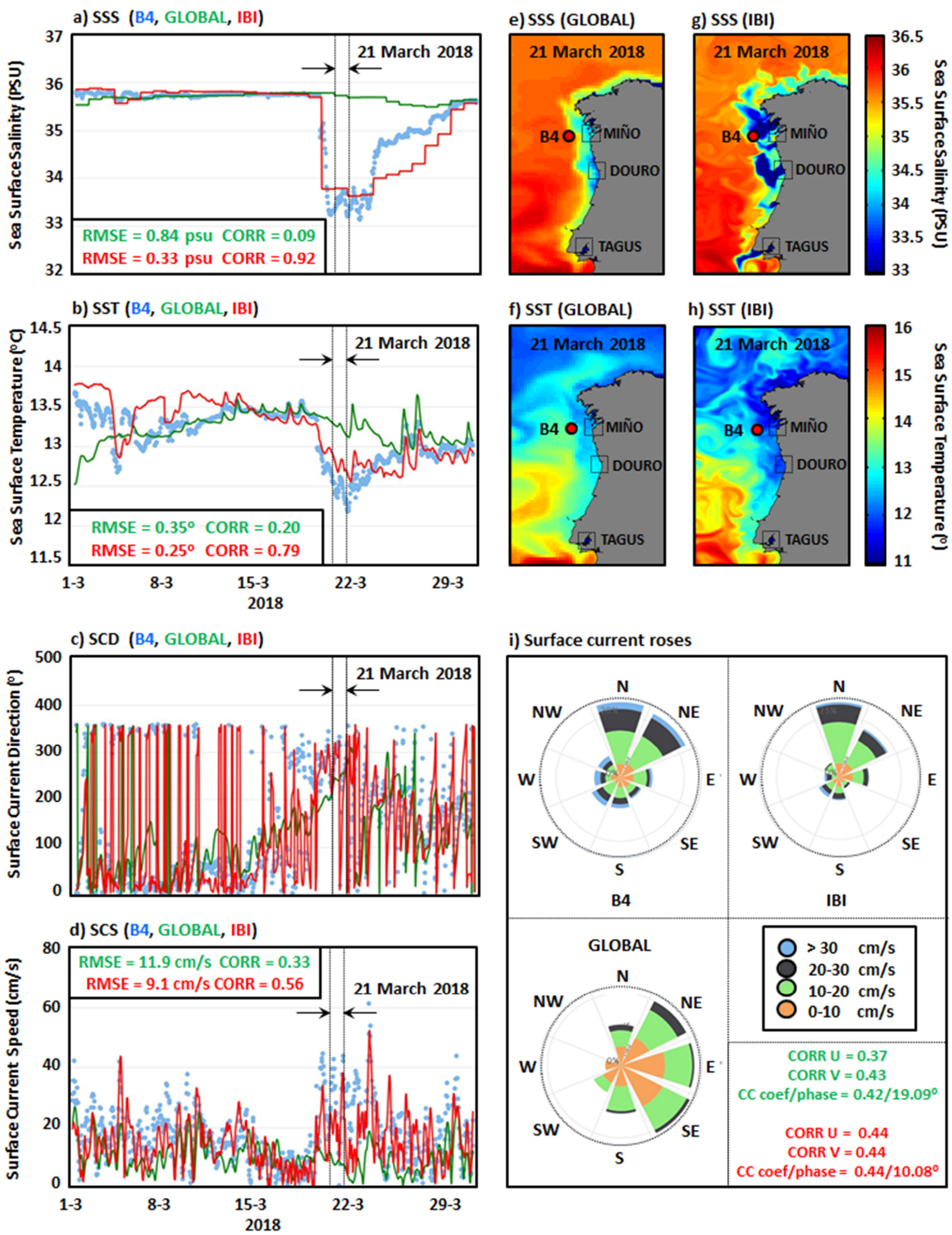

Figure 6. (a-d) Monthly inter-comparison (March 2018) between GLOBAL (green line), IBI (red line) and B4 buoy (blue dots): sea surface salinity (SSS), temperature (SST), current direction (SCD) and current speed (SCS); (e-f) Daily maps of SSS and SST derived from GLOBAL outputs for the 21st of March. Red filled dot represents B4 buoy location; (g-h) Daily maps of SSS and SST derived from IBI outputs for the 21st of March; (i) Monthly surface current roses. Monthly skill metrics derived from model-observation comparisons are provided.

Ocean Sci. Discuss., https://doi.org/10.5194/os-2018-168
Manuscript under review for journal Ocean Sci.
Discussion started: 17 January 2019

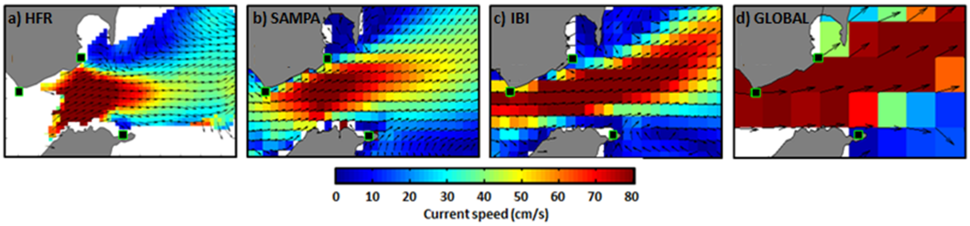

Figure 7. Annual mean circulation pattern in GIBST for 2017, derived from hourly estimations provided by: a) HFR; b) SAMPA coastal model; c) IBI regional model; d) GLOBAL model. For the sake of clarity, only one vector every two was plotted in HFR map.

Ocean Sci. Discuss., https://doi.org/10.5194/os-2018-168
Manuscript under review for journal Ocean Sci.
Discussion started: 17 January 2019

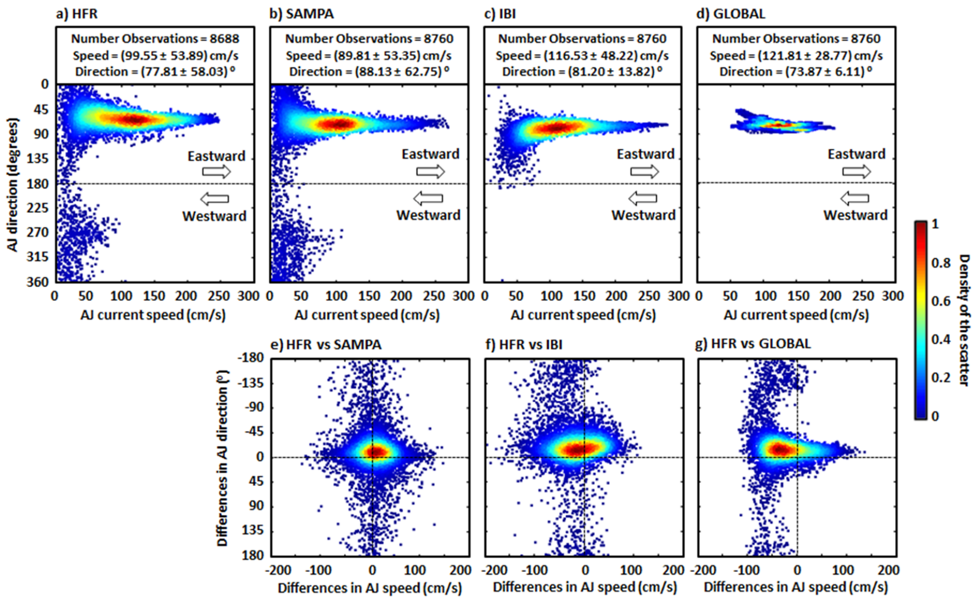

Figure 8. (a-d) Annual (2017) scatter plot of hourly AJ current speed versus direction (angle measured clockwise from the North); estimations provided by: a) HFR; b) SAMPA; c) IBI; d) GLOBAL. Mean and standard deviation values of both AJ speed and direction are gathered in black boxes; (e-g) Annual scatter plot of differences (observation minus model) in AJ speed and direction between: e) HFR and SAMPA; f) HFR and IBI; g) HFR and GLOBAL.

Ocean Sci. Discuss., https://doi.org/10.5194/os-2018-168
Manuscript under review for journal Ocean Sci.
Discussion started: 17 January 2019

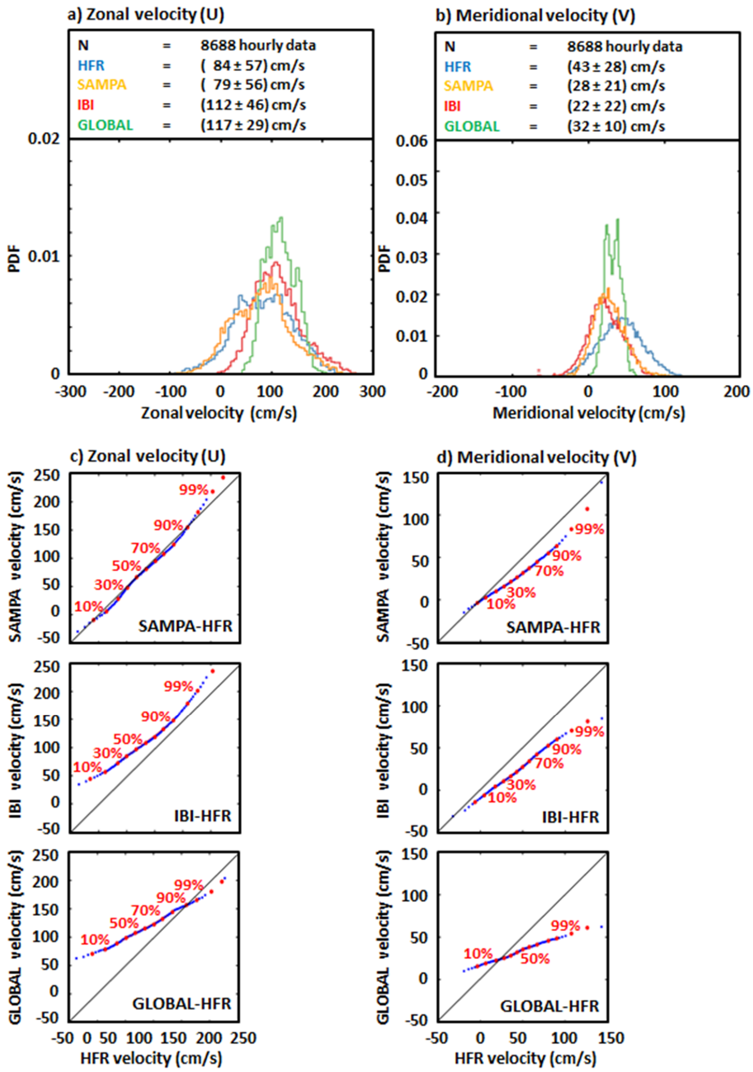

Figure 9. Annual (2017) histogram of hourly: (a) zonal current velocities; (b) meridional current velocities, as provided by HFR, SAMPA, IBI and GLOBAL. Mean and standard deviation values are gathered in black boxes. Quantile-quantile plots of hourly: (c) zonal current velocities; (d) meridional current velocities, as derived from the observation-model comparison. 10–99% quantiles were established (red filled dots);

Ocean Sci. Discuss., https://doi.org/10.5194/os-2018-168
Manuscript under review for journal Ocean Sci.
Discussion started: 17 January 2019

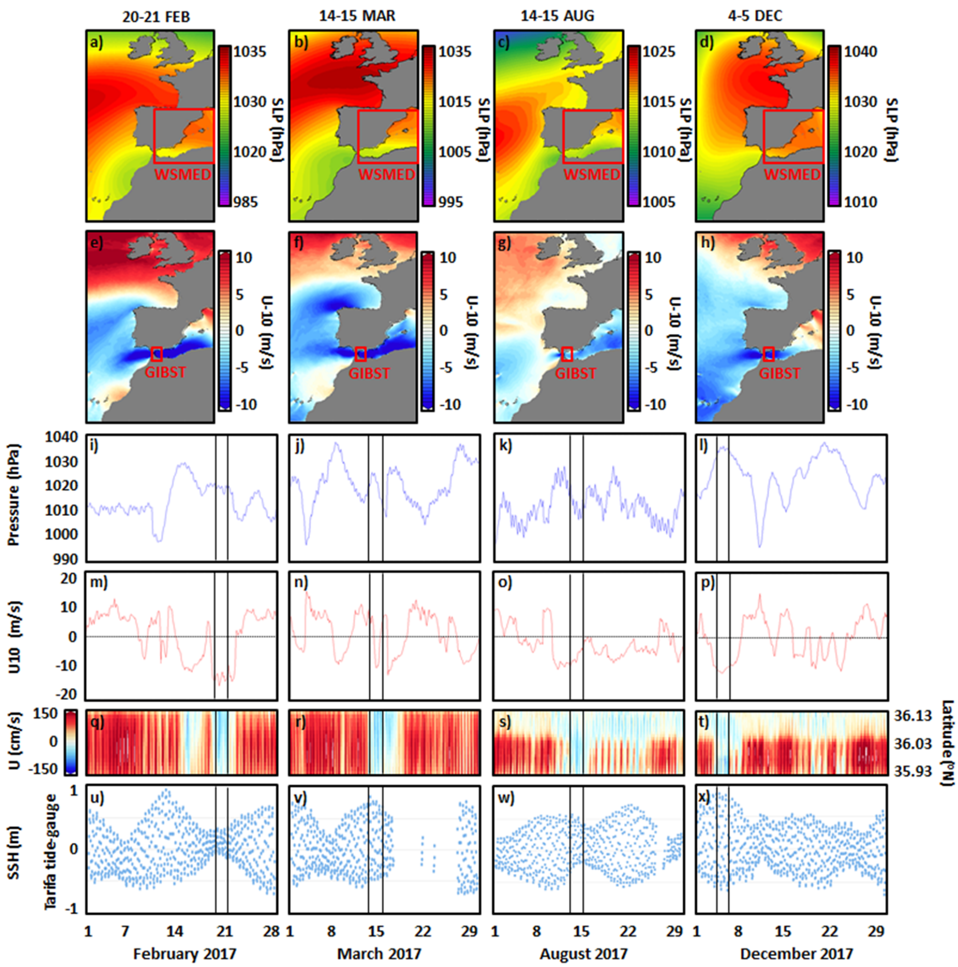

Figure 10. 2-day averaged synoptic maps of: (a-d) sea level pressure (SLP); (e-h) zonal wind at 10 m height (U-10), provided by ECMWF, corresponding to each of the four Atlantic inflow reversal events analysed during 2017. (i-l) Monthly time series of SLP, spatially averaged over the Western Mediterranean (WSMED) subregion, marked with a big red box in the maps of the first row; (m-p) Monthly time series of U-10, spatially averaged over the Strait of Gibraltar (GIBST) subregion, marked with a small red box in the maps of the second row; (q-t) Monthly Hovmöller diagrams of HFR-derived zonal current velocity at the selected transect. Red (blue) colour represent eastward (westward) flow; (u-x) Monthly time series of hourly sea surface height (SSH) provided by Tarifa tide-gauge, represented by a blue dot in Figure 1-c. 2-day episodes of permanent flow reversal are marked with black boxes in (i-x).

Ocean Sci. Discuss., https://doi.org/10.5194/os-2018-168
Manuscript under review for journal Ocean Sci.
Discussion started: 17 January 2019

Ocean Science
Discussions

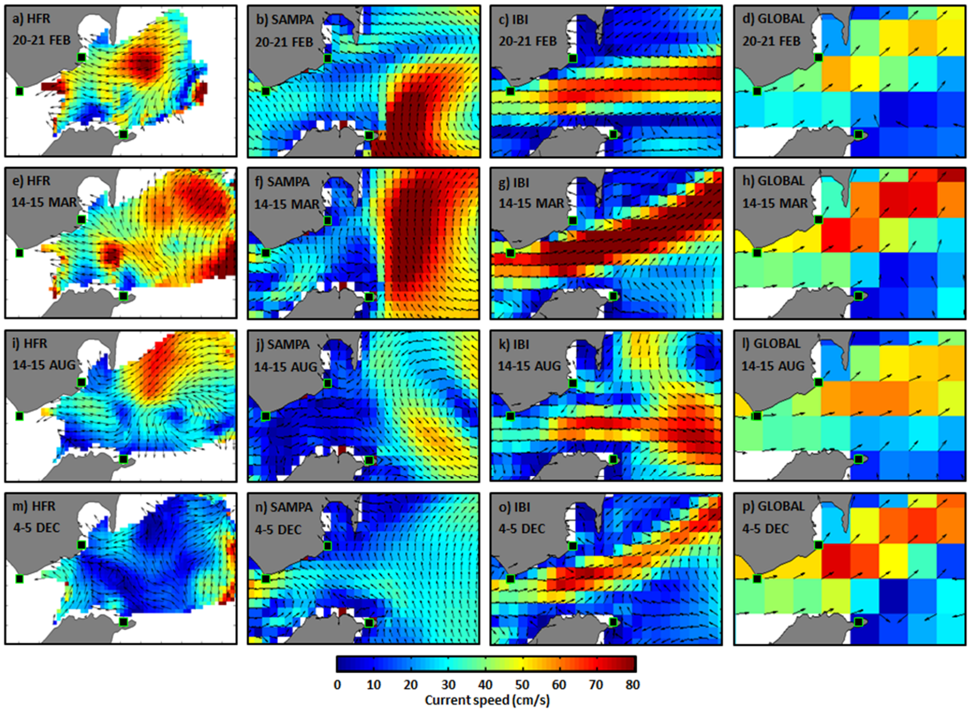

Figure 11. 2-day averaged maps of the surface circulation in GIBST, corresponding to each of the four Atlantic inflow reversal events detected in 2017 (from top to bottom). Maps derived from hourly estimations were provided by (from left to right): HFR, SAMPA coastal model, IBI regional model and GLOBAL model. For the sake of clarity, only one vector every two was plotted in HFR map.

Ocean Sci. Discuss., https://doi.org/10.5194/os-2018-168
Manuscript under review for journal Ocean Sci.
Discussion started: 17 January 2019

Ocean Science
Discussions
Open Access

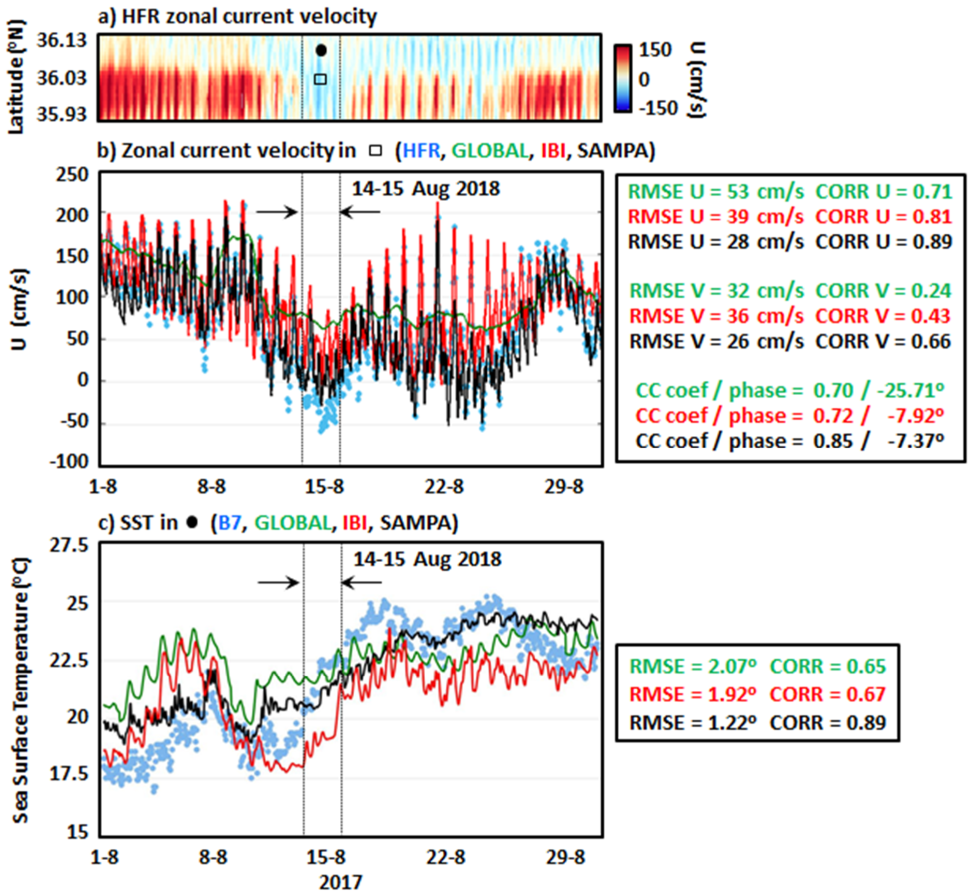

Figure 12. a) Monthly Hovmöller diagram of HFR-derived zonal current velocity at the selected transect in the Strait of Gibraltar for August 2017. Red (blue) colour represent eastward (westward) flow. A complete Atlantic inflow reversal episode marked with black box for the 14-15 August; b) Monthly times eries of zonal current velocity at the midpoint of the transect (represented by a black square in the Hovmöller diagram) provided by HFR (blue dots), SAMPA (black line), IBI (red line) and GLOBAL (green line); c) Monthly time series of SST at B7 buoy location (represented by a solid black dot in the Hovmöller diagram) provided by B7 buoy (blue dots), SAMPA (black line), IBI (red line) and GLOBAL (green line). Monthly skill metrics derived from observation-model comparison are gathered in black boxes on the right.

Ocean Sci. Discuss., https://doi.org/10.5194/os-2018-168
Manuscript under review for journal Ocean Sci.
Discussion started: 17 January 2019

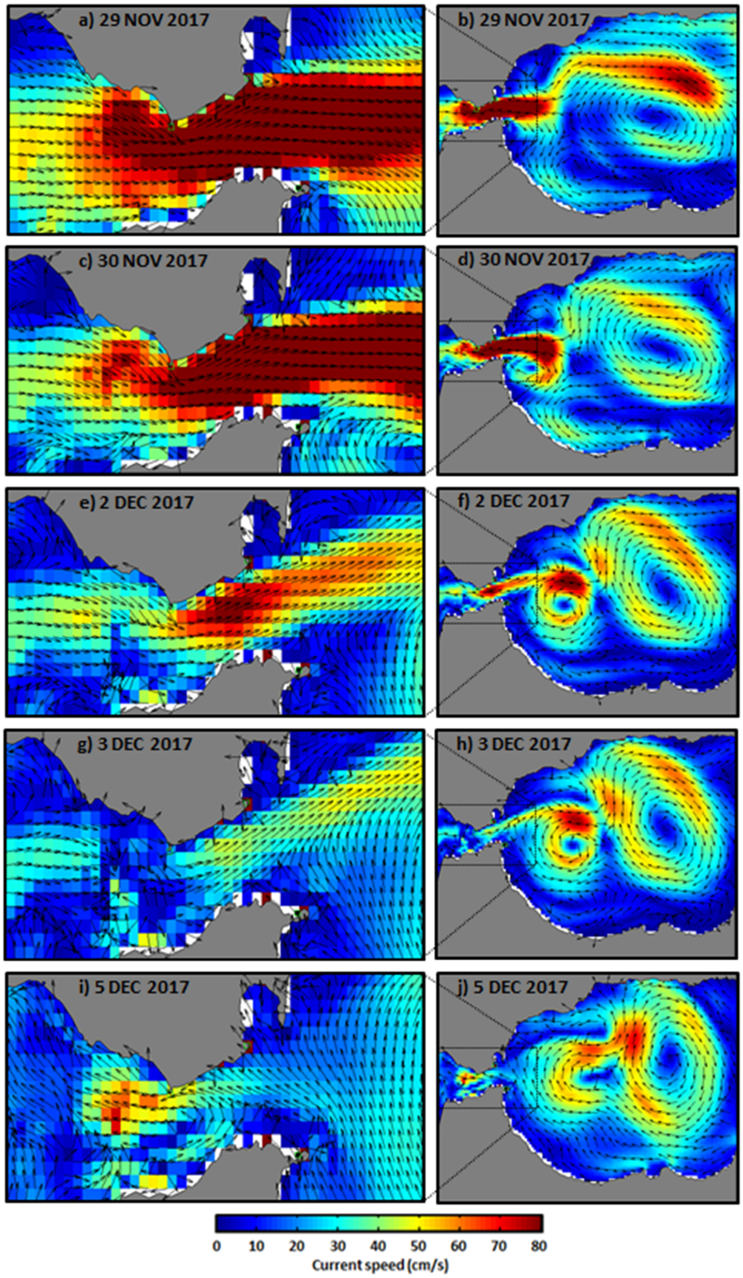

Figure 13. Sequence of SAMPA daily surface circulation maps covering the period from the 29th of November to the 5th of December 2017. General map on the right and zoom over the Strait of Gibraltar on the left. An inflow reversal through the narrowest section of the Strait of Gibraltar is evidenced by the 5th of December, as a result of a change in the wind regime, from westerlies to easterlies.

Ocean Sci. Discuss., https://doi.org/10.5194/os-2018-168
Manuscript under review for journal Ocean Sci.
Discussion started: 17 January 2019

Ocean Science
Discussions
Open Access
EGU

Features \ Model	CMEMS GLOBAL	CMEMS IBI	SAMPA
Model	NEMO 3.1	NEMO 3.6	MITgcm
Configuration	Global	Regional	Coastal
Domain: lon, lat	180°W-180°E, 89°S-90°N	19°W-5°E, 26°N-56°N	7.4°W-3°W, 35°N-37.2°N
Resolution	1/12°	1/36°	Variable (300-500 m at GIBST)
Product grid points	4320 x 2041	865 x 1081	200 x 100
Forecast (days)	10	5	3
Forecast update	Daily	Daily	Daily
Depth levels	50 (unevenly distributed)	50 (unevenly distributed)	46 (unevenly distributed)
Initial conditions	EN4 climatology	GLOBAL	IBI + NIVMAR
Open boundary conditions	NO	Daily 3D data from CMEMS GLOBAL	Daily 3D data from CMEMS IBI + barotropic velocity from NIVMAR
Atmospheric forcing	ECMWF (3-h)	ECMWF (3-h)	AEMET (1-h)
Rivers forcing	Monthly climatology	Climatology + Previmer + SMHI	NO
Tidal forcing	NO	11 tidal harmonics from FES2004 and TPXO7.1 models	8 tidal harmonics from FES2004 (MOG2D model)
Assimilation	YES (SAM2)	NO*	NO
Bathymetry	ETOPO1 + GEBCO8	ETOPO1 + GEBCO8	IOC + high resolution charts

Table 1. Basic features of the ocean forecast systems employed in the present study. * The operational version of IBI here used with spectral nudging. Assimilation scheme SAM2 was later introduced in v4 (April 2018).

Buoy	Model	Year	Location: lon, lat	Subregion	Depth (m)	Sampling
B1	WaveScan	2008	9.07ºW, 54.67ºN	IBISR	72	1 h
B2	WaveScan	2008	5.42ºW, 53.47ºN	IRISH	95	1 h
B3	SeaWatch	1990	3.09ºW, 43.64ºN	NIBSH	870	1 h
B4	SeaWatch	1998	9.43ºW, 42.12ºN	WIBSH	600	1 h
B5	SeaWatch	2004	1.47ºE, 40.68ºN	WSMED	688	1 h
B6	SeaWatch	1996	6.96ºW, 36.48ºN	CADIZ	450	1 h
B7	WatchKeeper	2010	5.42ºW, 36.07ºN	GIBST	40	1 h
B8	Triaxys	1992	15.39ºW, 28.05ºN	ICANA	30	1 h

Table 2. Description of the network of directional buoys used in this work. Year label stands for year of deployment. Subregions are defined in Figure 1-a.

Metrics \ HFR vs:	GLOBAL	IBI	SAMPA
Bias U (cm·s^{-1})	-32.98	-28.25	4.17
RMSD U (cm·s^{-1})	52.89	50.89	33.58
CORR U	0.71	0.68	0.83
Slope U	0.37	0.55	0.82
Intercept U (cm·s^{-1})	85.93	65.46	10.77
Bias V (cm/s)	10.52	20.32	15.19
RMSD V (cm·s^{-1})	30.57	36.09	28.48
CORR V	0.15	0.33	0.56
Slope V	0.05	0.26	0.41
Intercept V (cm·s^{-1})	29.98	11.27	10.17
Complex CORR	0.67	0.62	0.79
Phase (º)	-22.72	-12.68	-7.86

Table 3. Skill metrics derived from the 1-year (2017) validation of sea surface currents estimated by three operational forecasting systems against HFR-derived observations at the midpoint of the selected transect in the Strait of Gibraltar (Figure 1, c).